SIAM J. NUMER. ANAL.
Vol. 58, No. 5, pp. 2632–2661
© 2020 Society for Industrial and Applied Mathematics

A PRIMAL-DUAL WEAK GALERKIN FINITE ELEMENT METHOD FOR FOKKER–PLANCK TYPE EQUATIONS*

CHUNMEI WANG† AND JUNPING WANG‡

Abstract. This paper presents a primal-dual weak Galerkin finite element method for a class of second order elliptic equations of Fokker–Planck type. The method is based on a variational form where all the derivatives are applied to the test functions so that no regularity is necessary for the exact solution of the model equation. The numerical scheme is designed by using locally constructed weak second order partial derivatives and the weak gradient commonly used in the weak Galerkin context. Optimal order of convergence is derived for the resulting numerical solutions. Numerical results are reported to demonstrate the performance of the numerical scheme.

Key words. primal-dual, weak Galerkin, finite element methods, Fokker–Planck equation, weak Hessian, weak gradient, polytopal partitions

AMS subject classifications. Primary, 65N30, 65N15, 65N12, 74N20; Secondary, 35B45, 35J50, 35J35

DOI. 10.1137/17M1126618

1. Introduction.

The Fokker–Planck equation plays a critical role in statistical physics and in the study of fluctuations in physical and biological systems [16, 29, 31, 34, 18]. In statistical physics, it is a second order partial differential equation that describes the time evolution of the probability density function of the velocity of a particle under the influence of drag forces and random forces resulting from Gaussian white noise. The general setting of the Fokker–Planck equation is as follows. Given an open domain $\Omega \subset \mathbb{R}^d$ (the d-dimensional Euclidean space) and a terminal time T, we seek a time-dependent density function $p = p(x,t) :\ \Omega \times [0,T] \to \mathbb{R}$ satisfying

$$\begin{aligned} \partial_t p + \nabla \cdot (\boldsymbol{\mu} p) - \frac{1}{2} \sum_{i,j=1}^{d} \partial_{ij}^2 (a_{ij} p) &= 0, \qquad t \in (0,T),\ x \in \Omega, \\ p(x,0) &= p_0(x), \qquad x \in \Omega, \end{aligned} \tag{1.1}$$

where $\partial_{ij}^2 = \frac{\partial}{\partial x_j} \frac{\partial}{\partial x_i}$ is the second order partial derivative in the directions x_i and x_j, $a(x) = \{a_{ij}(x)\}_{d\times d}$ is the diffusion tensor, $\boldsymbol{\mu} = (\mu_1, \ldots, \mu_d)$ is the drift vector, and $p_0 = p_0(x)$ is the initial profile of the density function. Two common boundary conditions for (1.1) can be imposed: Dirichlet for the density function and Neumann condition for the flux. Homogeneous Dirichlet boundary data corresponds to the case where particles exit once they reach the boundary, and a prescribed flow or Neumann

*Received by the editors April 21, 2017; accepted for publication (in revised form) April 24, 2018; published electronically September 23, 2020.

https://doi.org/10.1137/17M1126618

Funding: The work of the first author was partially supported by National Science Foundation Award DMS-1849483. The work of the second author was supported by the NSF IR/D program, while working at National Science Foundation. However, any opinion, finding, and conclusions or recommendations expressed in this material are those of the author and do not necessarily reflect the views of the National Science Foundation.

†Department of Mathematics, Texas Tech University, Lubbock, TX 79409 (chunmei.wang@ttu.edu).

‡Division of Mathematical Sciences, National Science Foundation, 2415 Eisenhower Avenue, Alexandria, VA 22314 (jwang@nsf.gov).

Copyright © by SIAM. Unauthorized reproduction of this article is prohibited.

Downloaded 12/18/20 to 59.64.129.2. Redistribution subject to SIAM license or copyright; see https://epubs.siam.org/page/terms

boundary condition represents a known current of particles crossing the boundary in the normal direction.

For a smooth diffusion tensor, the second order differential part of the Fokker–Plank equation can be reformulated as

$$\frac{1}{2}\partial_{ij}^2(a_{ij}p) = \frac{1}{2}\partial_j(a_{ij}\partial_i p) + \frac{1}{2}\partial_j((\partial_i a_{ij})p). \tag{1.2}$$

Therefore, (1.1) can be viewed as a time-evolving convection-diffusion equation in divergence form, and the corresponding Fokker–Planck equation is considered as a relatively less challenging problem to solve numerically. But for the nonsmooth diffusion tensor, the formulation (1.2) is no longer valid as the coefficients $\{a_{ij}\}$ are not differentiable. In fact, it can be seen that for nonsmooth diffusion tensor $a(x)$, the resulting probability density function $p = p(x)$ exhibits discontinuities that are unknown a priori so that numerical solutions are not only necessary but also difficult to obtain in practical applications.

Numerical methods for the Fokker–Planck equation (1.1) involve discretization in both time and spatial directions. As is well known in numerical parabolic research [43], the convergence theory of numerical methods for parabolic equations often makes use of properly defined Ritz projections arising from the differential operators in the spatial variables. For the Fokker–Planck equation, the Ritz projection would be a numerical protocol for the following second order elliptic equation in nondivergence or double-divergence form: find an unknown function $u = u(x)$ such that

$$\begin{aligned} -\frac{1}{2}\sum_{i,j=1}^{d}\partial_{ij}^2(a_{ij}u) + \nabla\cdot(\boldsymbol{\mu}u) &= f \quad \text{in } \Omega, \\ u &= 0 \quad \text{on } \partial\Omega, \end{aligned} \tag{1.3}$$

where $\partial\Omega$ is the boundary of the domain, and $f \in L^2(\Omega)$ is a given square integrable function. The goal of this paper is to develop new finite element methods and their corresponding convergence theory for the model problem (1.3) by using the primal-dual approach first introduced in [39]. It should be emphasized that we are concerned with the equations where no smoothness assumptions are made on the coefficients so that the exact solution possesses discontinuities. The solution discontinuity imposes a grand challenge on the numerical solutions that are stable and accurate. Our paper is in response to this challenge and intends to offer some promising approaches.

Various finite element methods have been designed for the Fokker–Planck equation for a numerical computation of the probability density function; see [3, 23, 24, 2, 33, 27, 22] and the references cited therein. In [3, 23], the stationary Fokker–Planck equation was discretized by using Galerkin finite element methods based on a weak form obtained from the usual integration by parts. In [24], another Galerkin finite element method was used to solve the Fokker–Planck equation in combination with a generalized Lagrange multiplier method to handle the associated integral constraint. In [2], the authors applied the usual C^0 finite element method to the Fokker–Planck system subject to both additive and multiplicative white noise excitations. In [27], the authors developed a framework for multiscale finite element methods for the solution of the multidimensional Fokker–Planck equation in stochastic structural dynamics. All the aforementioned finite element methods assumed smooth or constant diffusion tensor $a(x)$ for the Fokker–Planck equation so that a regular weak form can be derived for the system. In [22], a C^0 finite element scheme was described and numerically tested for the transient Fokker-Planck equation without any smoothness assumption

Copyright © by SIAM. Unauthorized reproduction of this article is prohibited.

Downloaded 12/18/20 to 59.64.129.2. Redistribution subject to SIAM license or copyright; see https://epubs.siam.org/page/terms

on $a(x)$, but no theory of convergence was developed for the corresponding numerical method.

The paper is organized as follows. In section 2, we review some basic results for second order elliptic PDEs in nondivergence form. A new result on solution existence and uniqueness is derived in this section for elliptic operators with first order terms (drift vector). This section also illustrates the motivation of the primal-dual weak Galerkin finite element method. In section 3, we shall briefly discuss the computation of weak gradients and weak second order partial derivatives. In section 4, we present a detailed description of the primal-dual weak Galerkin finite element method for the Fokker–Planck type model problem (1.3) based on the weak formulation (2.3). Section 5 is dedicated to a study of the new algorithm on the solution existence and uniqueness. In section 6, we shall derive an error equation satisfied by the numerical solutions and a properly defined projection of the exact solution. Then in section 7, we establish an error estimate for the primal variable that is of optimal order in $L^2(\Omega)$—the space of square integrable functions over Ω. In section 8, we shall discuss a C^0-conforming element with reduced degree of freedoms in the finite element space. The computational complexity of the general scheme is also briefly discussed in this section. Section 9 contains some estimates for the L^2 projection of piecewise smooth functions. Finally in section 10, we report some numerical results to demonstrate the performance of the primal-dual weak Galerkin finite element algorithm.

2. Preliminaries. We will follow the usual notation for Sobolev spaces and norms [11, 19, 21, 20, 4]. For any open bounded domain $D \subset \mathbb{R}^d$ with Lipschitz continuous boundary, we use $\|\cdot\|_{s,D}$ and $|\cdot|_{s,D}$ to denote the norm and seminorms in the Sobolev space $H^s(D)$ for any $s \geq 0$, respectively. The inner product in $H^s(D)$ is denoted by $(\cdot,\cdot)_{s,D}$. The space $H^0(D)$ coincides with $L^2(D)$, for which the norm and the inner product are denoted by $\|\cdot\|_D$ and $(\cdot,\cdot)_D$, respectively. When $D = \Omega$, we shall drop the subscript D in the norm and inner product notation. For convenience, we use "$\lesssim$" to denote "less than or equal to up to a general constant independent of the meshsize or functions appearing in the inequality."

2.1. Analysis of the PDE. Denote by $\mathcal{L}$ the bounded linear operator from $H^2(\Omega)$ to $L^2(\Omega)$ defined by

$$\mathcal{L}v := \frac{1}{2}\sum_{i,j=1}^{d} a_{ij}\partial^2_{ji}v + \boldsymbol{\mu}\cdot\nabla v, \qquad v \in H^2(\Omega), \tag{2.1}$$

where it is assumed that $a_{ij} = a_{ji} \in L^\infty(\Omega)$ for $i,j = 1,\ldots,d$ and that the diffusion tensor $a(x)$ is uniformly elliptic, i.e., there exist positive constants α_1 and α_2 such that

$$\alpha_1|\xi|^2 \leq \sum_{i,j=1}^{d} a_{ij}\xi_i\xi_j \leq \alpha_2|\xi|^2 \qquad \forall \xi = (\xi_1,\ldots,\xi_d)^T \in \Omega. \tag{2.2}$$

We further assume that the drift vector $\boldsymbol{\mu} \in (L^\infty(\Omega))^d$.

By a *weak solution* of (1.3) we mean a function $u = u(x) \in L^2(\Omega)$ satisfying

$$(u, \mathcal{L}v) = -(f, v) \qquad \forall v \in H^2(\Omega) \cap H^1_0(\Omega). \tag{2.3}$$

For the problem (2.3) to be well posed, the differential operator $\mathcal{L}$ is assumed to satisfy the H^2-regularity property in the sense that for any given $\chi \in L^2(\Omega)$, there exists a unique strong solution $\Phi \in H^2(\Omega) \cap H^1_0(\Omega)$ satisfying

Copyright © by SIAM. Unauthorized reproduction of this article is prohibited.

Downloaded 12/18/20 to 59.64.129.2. Redistribution subject to SIAM license or copyright; see https://epubs.siam.org/page/terms

$$\mathcal{L}\Phi = \chi, \qquad \|\Phi\|_2 \lesssim \|\chi\|. \tag{2.4}$$

In [36], it was shown that if $\boldsymbol{\mu} = 0$, $d = 2$, and the boundary of the domain Ω is sufficiently smooth, then there exists exactly one solution for $\mathcal{L}\Phi = \chi$ vanishing on the boundary and satisfying the regularity estimate of (2.4). However, the situation is completely different for problems in higher dimensions. For example, the solution uniqueness breaks down when $d \geq 3$ for coefficients $a(x)$ that are in L^∞ but not continuous. One such counterexample is given by

$$a(x) = I_{d\times d} + \frac{(d+\lambda-2)xx^T}{(1-\lambda)|x|^2} \tag{2.5}$$

on the unit ball $\Omega = B_1(0)$ with $d > 2(2-\lambda)$, as it can be seen that $\Phi = |x|^\lambda - 1 \in H^2(\Omega) \cap H_0^1(\Omega)$ satisfies $\mathcal{L}\Phi = 0$ when $\boldsymbol{\mu} = 0$.

The H^2-regularity result for the differential operator $\mathcal{L}$ with $\boldsymbol{\mu} = 0$ was extended to a special class of second order elliptic equations in nondivergence form introduced by Cordès [13]. The differential operator $\mathcal{L}$ is of the Cordès type if the eigenvalues of the matrix $a(x)$ are not too dispersed, more precisely, if there exists an $\varepsilon \in (0, 1]$ such that

$$\left(\sum_{i=1}^d a_{ii}\right)^2 \geq (d-1+\varepsilon)\sum_{i,j=1}^d a_{ij}^2 \qquad \text{in } \Omega. \tag{2.6}$$

In [35], it was proved that, under the assumption of (2.2) and (2.6), for every $\chi \in L^2(\Omega)$, the equation $\mathcal{L}\Phi = \chi$ (with $\boldsymbol{\mu} = 0$) has exactly one solution in $H^2(\Omega)$ with vanishing boundary value, provided that the boundary of Ω is sufficiently smooth and has mean curvature of constant sign. This result was extended to bounded convex domains in [32] under the very same assumption of the Cordès condition. It should be noted that the Cordès condition (2.6) is automatically satisfied in two dimensions for a diffusion tensor that is bounded, symmetric, and uniformly positive definite in the domain (see [39] for a verification).

For the differential operator $\mathcal{L}$ with nonvanishing drift vector $\boldsymbol{\mu} \neq 0$ and discontinuous diffusion tensor $a(x)$, we were not able to find any result on the H^2-regularity estimate (2.4) in the existing literature. But one may derive some regularity results by using the usual perturbation argument. The following is a result for the linear operator $\mathcal{L}$ with small but nonvanishing drift vector $\boldsymbol{\mu}$.

THEOREM 2.1. *Let $\Omega \subset \mathbb{R}^d$ be a bounded convex domain, and let the differential operator $\mathcal{L}$ defined in* (2.1) *satisfy $a(x) \in [L^\infty(\Omega)]^{d\times d}$, $\boldsymbol{\mu} \in [L^\infty(\Omega)]^d$, the ellipticity condition* (2.2)*, and the Cordès condition* (2.6)*. Then, for any given $\chi \in L^2(\Omega)$, there exists a unique $\Phi \in H^2(\Omega) \cap H_0^1(\Omega)$ that is a strong solution of $\mathcal{L}\Phi = \chi$, and this strong solution satisfies*

$$\|\Phi\|_2 \lesssim \|\chi\|_0,$$

provided that the drift vector is sufficiently small such that $\|\mathcal{L}_0^{-1}\|\|\boldsymbol{\mu}\|_\infty < 1$. Here $\mathcal{L}_0 := \frac{1}{2}\sum_{i,j=1}^d a_{ij}\partial_{ji}^2 v$ is the principle part of $\mathcal{L}$ and

$$\|\mathcal{L}_0^{-1}\| = \sup_{f\in L^2(\Omega), \|f\|_0=1} \|\mathcal{L}_0^{-1} f\|_2.$$

Proof. For bounded convex domain Ω, it has been proved that the operator $\mathcal{L}_0$ is an isomorphism from $H^2(\Omega) \cap H_0^1(\Omega)$ to $L^2(\Omega)$ provided that (2.2) and (2.6) are

Copyright © by SIAM. Unauthorized reproduction of this article is prohibited.

Downloaded 12/18/20 to 59.64.129.2. Redistribution subject to SIAM license or copyright; see https://epubs.siam.org/page/terms

Downloaded 12/18/20 to 59.64.129.2. Redistribution subject to SIAM license or copyright; see https://epubs.siam.org/page/terms

satisfied. For any $v \in H^2(\Omega) \cap H_0^1(\Omega)$, denote by $T(v)$ the solution of the following problem:

$$\begin{aligned} \mathcal{L}_0 T(v) + \boldsymbol{\mu} \cdot \nabla v &= \chi \qquad \text{in } \Omega, \\ T(v) &= 0 \qquad \text{on } \partial\Omega. \end{aligned} \tag{2.7}$$

It is clear that T maps $H^2(\Omega) \cap H_0^1(\Omega)$ to itself. Furthermore, for any two functions $v, w \in H^2(\Omega) \cap H_0^1(\Omega)$, from (2.7) we have

$$\mathcal{L}_0(T(v) - T(w)) + \boldsymbol{\mu} \cdot \nabla(v - w) = 0.$$

It follows that

$$\begin{aligned} \|T(v) - T(w)\|_2 &= \|\mathcal{L}_0^{-1}\mathcal{L}_0(T(v) - T(w))\|_2 \\ &\le \|\mathcal{L}_0^{-1}\|\|\mathcal{L}_0(T(v) - T(w))\|_0 \\ &\le \|\mathcal{L}_0^{-1}\|\|\boldsymbol{\mu} \cdot \nabla(v - w)\|_0. \end{aligned} \tag{2.8}$$

Now substituting

$$\|\boldsymbol{\mu} \cdot \nabla(v - w)\|_0 \le \|\boldsymbol{\mu}\|_\infty \|v - w\|_1$$

into (2.8) yields

$$\|T(v) - T(w)\|_2 \le \|\mathcal{L}_0^{-1}\|\|\boldsymbol{\mu}\|_\infty \|v - w\|_2. \tag{2.9}$$

It follows that T is a contraction mapping if the drift vector $\boldsymbol{\mu}$ is sufficiently small so that $\rho := \|\mathcal{L}_0^{-1}\|\|\boldsymbol{\mu}\|_\infty < 1$.

As a contraction mapping, T must have a fixed point $\Phi \in H^2(\Omega) \cap H_0^1(\Omega)$ that satisfies

$$\mathcal{L}_0 \Phi + \boldsymbol{\mu} \cdot \nabla \Phi = \chi \qquad \text{in } \Omega,$$

which is precisely $\mathcal{L}\Phi = \chi$. For this fixed point, the following estimate holds true:

$$\begin{aligned} \|\Phi\|_2 &= \|\mathcal{L}_0^{-1}\mathcal{L}_0\Phi\|_2 \\ &\le \|\mathcal{L}_0^{-1}\|\|\mathcal{L}_0\Phi\|_0 \\ &\le \|\mathcal{L}_0^{-1}\|\|\chi - \boldsymbol{\mu} \cdot \nabla\Phi\|_0 \\ &\le \|\mathcal{L}_0^{-1}\|\|\chi\|_0 + \|\mathcal{L}_0^{-1}\|\|\boldsymbol{\mu}\|_\infty\|\Phi\|_2 \\ &\le \|\mathcal{L}_0^{-1}\|\|\chi\|_0 + \rho\|\Phi\|_2, \end{aligned} \tag{2.10}$$

which leads to

$$(1 - \rho)\|\Phi\|_2 \le \|\mathcal{L}_0^{-1}\|\|\chi\|_0.$$

This completes the proof of the theorem. ∎

Throughout the paper, the domain Ω and the differential operator $\mathcal{L}$ are assumed to satisfy the H^2-regularity estimate (2.4) so that the formulation (2.3) is well defined.

2.2. Motivation of numerics. Our numerical scheme for the model problem (1.3) is based on the weak formulation (2.3) through a weak Galerkin approach that combines the primal variable with its dual. The dual problem for the primal equation (2.3) is given by

$$(w, \mathcal{L}\rho) = 0 \qquad \forall w \in L^2(\Omega), \tag{2.11}$$

Copyright © by SIAM. Unauthorized reproduction of this article is prohibited.

Downloaded 12/18/20 to 59.64.129.2. Redistribution subject to SIAM license or copyright; see https://epubs.siam.org/page/terms

where $\rho \in H^2(\Omega) \cap H_0^1(\Omega)$ is the dual variable. Under the H^2-regularity assumption (2.4), the solution to the dual problem (2.11) is clearly trivial, i.e., $\rho \equiv 0$. Note that the primal and the dual equations are formally uncorrelated to each other in the continuous case, but this is changed significantly in the context of weak Galerkin finite element methods. In the weak Galerkin approach, the differential operator $\mathcal{L}$ is discretized as

$$\mathcal{L}_w(v) := \boldsymbol{\mu} \cdot \nabla_w v + \frac{1}{2} \sum_{i,j=1}^{d} a_{ij} \partial_{ji,w}^2 v,$$

where ∇_w is a discrete weak gradient [40, 25, 42, 41] and $\partial_{ji,w}^2$ is a discrete weak second order partial derivative [26, 37] (also see section 3 for their definition). The corresponding primal and dual equations then become

$$\text{discrete primal:} \quad (u_h, \mathcal{L}_w v) = -(f, v) \qquad \forall v \in V_{h,k}^0 \tag{2.12}$$

and

$$\text{discrete dual:} \quad (w, \mathcal{L}_w \rho_h) = 0 \qquad \forall w \in W_{h,s}, \tag{2.13}$$

where $V_{h,k}^0$ and $W_{h,s}$ are two weak finite element spaces associated with a prescribed finite element partition $\mathcal{T}_h$ used to approximate $H^2(\Omega) \cap H_0^1(\Omega)$ and $L^2(\Omega)$, respectively. While neither (2.12) nor (2.13) makes any computationally feasible schemes, their combination through the use of a carefully chosen stabilizer does provide numerical methods that are efficient, accurate, and stable for several model problems [8, 9, 7, 39]. The finite element space $V_{h,k}^0$ consists of piecewise polynomials defined on each element $T \in \mathcal{T}_h$ and the element boundary ∂T. Other finite element methods with similar features, but on different applications, include the hybridized formulation of the mixed finite element method [17], the hybridizable discontinuous Galerkin method [12], and the ultraweak methods for Helmholtz equations [15, 10, 6].

A formal description of the scheme reads as follows: find $u_h \in W_{h,s}$ and $\rho_h \in V_{h,k}^0$ such that

$$\begin{aligned} s(\rho_h, v) + (u_h, \mathcal{L}_w v) &= -(f, v) \qquad \forall v \in V_{h,k}^0, \\ (w, \mathcal{L}_w \rho_h) &= 0 \qquad \forall w \in W_{h,s}, \end{aligned} \tag{2.14}$$

where $s(\cdot, \cdot)$ is a bilinear form in $V_{h,k}^0 \times V_{h,k}^0$ known as *stabilizer* or *smoother* that enforces a certain weak continuity for the approximation ρ_h. Numerical schemes in the form of (2.14) were named *primal-dual weak Galerkin finite element methods* in [39], but were broadly called *stabilized finite element methods* in [8, 9, 7].

In the rest of the paper, we will provide all the technical details for the numerical scheme (2.14), including the construction of the finite element spaces $V_{h,k}^0$ and $W_{h,s}$, representation of the stabilizer or smoother $s(\cdot, \cdot)$, mathematical convergence for the corresponding numerical approximations, and some numerical results that demonstrate the performance of the method. One of the distinguished features of this approach lies in ultraweak regularity assumptions for the primal variable $u = u(x)$ in the mathematical convergence theory. The method essentially assumes no regularity on the primal variable so that solutions with discontinuity can be well approximated by our primal-dual finite element method. This work is a nontrivial extension of [39] in both theory and algorithmic development.

Copyright © by SIAM. Unauthorized reproduction of this article is prohibited.

Downloaded 12/18/20 to 59.64.129.2. Redistribution subject to SIAM license or copyright; see https://epubs.siam.org/page/terms

3. Weak partial derivatives. The goal of this section is to offer a brief definition and computation of the discrete weak partial derivatives introduced in [37, 38, 41]. To this end, let T be a polygonal or polyhedral region with boundary ∂T. By a weak function on T we mean a triplet $v = \{v_0, v_b, \mathbf{v}_g\}$ in which $v_0 \in L^2(T)$, $v_b \in L^2(\partial T)$ and $\mathbf{v}_g \in [L^2(\partial T)]^d$. The first and second components v_0 and v_b are intended for the value of v in the interior and on the boundary of T, respectively. The third component $\mathbf{v}_g = (v_{g1}, \ldots, v_{gd}) \in \mathbb{R}^d$ is used to represent the gradient of v on ∂T. In general, v_b and $\mathbf{v}_g$ are not required to be consistent with the trace of v_0 and ∇v_0 on ∂T. Denote by $\mathcal{W}(T)$ the space of all weak functions on T:

$$\mathcal{W}(T) = \left\{ v = \{v_0, v_b, \mathbf{v}_g\} : v_0 \in L^2(T), v_b \in L^2(\partial T), \mathbf{v}_g \in \left[L^2(\partial T)\right]^d \right\}. \tag{3.1}$$

For any $v \in \mathcal{W}(T)$, the weak second order partial derivative $\partial^2_{ij} v$, denoted as $\partial^2_{ij,w} v$, is defined as a linear functional in the dual space of $H^2(T)$ satisfying

$$\left(\left(\partial^2_{ij,w} v, \varphi\right)\right)_T = (v_0, \partial^2_{ji}\varphi)_T - \langle v_b n_i, \partial_j \varphi\rangle_{\partial T} + \langle v_{gi}, \varphi n_j\rangle_{\partial T} \tag{3.2}$$

for all $\varphi \in H^2(T)$. Here, $(\!(\chi, \varphi)\!)_T$ stands for the action of χ at $\varphi \in H^2(T)$, $\mathbf{n} = (n_1, \ldots, n_d)$ is the unit outward normal direction to ∂T, $(\cdot,\cdot)_T$ is the usual L^2 inner product in $L^2(T)$, and $\langle\cdot,\cdot\rangle_{\partial T}$ is the L^2 inner product in $L^2(\partial T)$.

The weak gradient of $v \in \mathcal{W}(T)$, denoted by $\nabla_w v$, is defined as a linear functional in the dual space of $[H^1(T)]^d$ such that

$$(\!(\nabla_w v, \boldsymbol{\psi})\!)_T = -(v_0, \nabla\cdot\boldsymbol{\psi})_T + \langle v_b, \boldsymbol{\psi}\cdot\mathbf{n}\rangle_{\partial T}$$

for all $\boldsymbol{\psi} \in [H^1(T)]^d$. Note that the weak gradient makes no use of the third component of the weak function v.

Denote by $P_r(T)$ the set of polynomials on T with degree no more than r. A discrete version of $\partial^2_{ij,w} v$ for $v \in \mathcal{W}(T)$, denoted by $\partial^2_{ij,w,r,T} v$, is defined as the unique polynomial in $P_r(T)$ satisfying

$$\left(\partial^2_{ij,w,r,T} v, \varphi\right)_T = \left(v_0, \partial^2_{ji}\varphi\right)_T - \langle v_b n_i, \partial_j\varphi\rangle_{\partial T} + \langle v_{gi}, \varphi n_j\rangle_{\partial T} \tag{3.3}$$

for all $\varphi \in P_r(T)$, which, by using integration by parts, yields

$$\left(\partial^2_{ij,w,r,T} v, \varphi\right)_T = \left(\partial^2_{ij} v_0, \varphi\right)_T + \langle (v_0 - v_b) n_i, \partial_j\varphi\rangle_{\partial T} - \langle \partial_i v_0 - v_{gi}, \varphi n_j\rangle_{\partial T} \tag{3.4}$$

for all $\varphi \in P_r(T)$.

A discrete form of $\nabla_w v$ for $v \in \mathcal{W}(T)$, denoted by $\nabla_{w,r,T} v$, is defined as the unique polynomial vector in $[P_r(T)]^d$ satisfying

$$(\nabla_{w,r,T} v, \boldsymbol{\psi})_T = -(v_0, \nabla\cdot\boldsymbol{\psi})_T + \langle v_b, \boldsymbol{\psi}\cdot\mathbf{n}\rangle_{\partial T} \quad \forall \boldsymbol{\psi} \in [P_r(T)]^d, \tag{3.5}$$

which, from integration by parts, gives

$$(\nabla_{w,r,T} v, \boldsymbol{\psi})_T = (\nabla v_0, \boldsymbol{\psi})_T - \langle v_0 - v_b, \boldsymbol{\psi}\cdot\mathbf{n}\rangle_{\partial T} \quad \forall \boldsymbol{\psi} \in [P_r(T)]^d, \tag{3.6}$$

provided that v_0 is sufficiently regular.

4. Numerical schemes. The goal of this section is to present a finite element method for the variational problem (2.3). To this end, let $\mathcal{T}_h$ be a finite element partition of the domain Ω into polygons in two dimensions or polyhedra in three dimensions

Copyright © by SIAM. Unauthorized reproduction of this article is prohibited.

Downloaded 12/18/20 to 59.64.129.2. Redistribution subject to SIAM license or copyright; see https://epubs.siam.org/page/terms

which is shape regular in the sense as described in [41]. For three-dimensional domains, all the polyhedral elements are assumed to have flat faces. Denote by $\mathcal{E}_h$ the set of all edges or faces in $\mathcal{T}_h$ and $\mathcal{E}_h^0 = \mathcal{E}_h \setminus \partial\Omega$ the set of all interior edges or faces. Denote by h_T the meshsize of $T \in \mathcal{T}_h$ and $h = \max_{T\in\mathcal{T}_h} h_T$ the meshsize of the partition $\mathcal{T}_h$.

Let $k \geq 1$ be a given integer. Denote by $V_k(T)$ the discrete local weak function space on T given by

$$V_k(T) = \{\{v_0, v_b, \mathbf{v}_g\} : \quad v_0 \in P_k(T),\ v_b \in P_k(e),\ \mathbf{v}_g \in [P_{k-1}(e)]^d,\ e \subset \partial T\}.$$

By patching $V_k(T)$ over all the elements $T \in \mathcal{T}_h$ through a common value v_b and $\mathbf{v}_g$ on the interior edges/faces, we obtain a global weak finite element space $V_{h,k}$:

$$V_{h,k} = \big\{\{v_0, v_b, \mathbf{v}_g\} : \quad \{v_0, v_b, \mathbf{v}_g\}|_T \in V_k(T),\ T \in \mathcal{T}_h\big\}.$$

Denote by $V_{h,k}^0$ the subspace of $V_{h,k}$ with vanishing boundary value for v_b on $\partial\Omega$, i.e.,

$$V_{h,k}^0 = \big\{\{v_0, v_b, \mathbf{v}_g\} \in V_{h,k} : \quad v_b|_e = 0,\ e \subset \partial\Omega\big\}.$$

For any given integer $s \geq 0$, denote by $W_{h,s}$ the usual finite element space consisting of piecewise polynomials of degree s, i.e.,

$$W_{h,s} = \{w : \quad w|_T \in P_s(T),\ T \in \mathcal{T}_h\}.$$

For application in the approximation of (2.3), the integer s will be chosen as either $s = k-1$ or $s = k-2$. In the case of $k = 1$, the only viable option for this integer would be $s = 0$.

For simplicity of notation, denote by $\nabla_w\sigma$ the discrete weak gradient $\nabla_{w,k-1,T}\sigma$ computed by using (3.5) on each element T with $r = k-1$:

$$(\nabla_w\sigma)|_T = \nabla_{w,k-1,T}(\sigma|_T), \qquad \sigma \in V_{h,k}.$$

Analogously, we use $\partial^2_{ij,w}\sigma$ to denote the discrete weak second order partial derivative $\partial^2_{ij,w,s,T}\sigma$ computed by using (3.3) on each element T with $r = s$:

$$\left(\partial^2_{ij,w}\sigma\right)|_T = \partial^2_{ij,w,s,T}(\sigma|_T), \quad \sigma \in V_{h,k}.$$

The corresponding weak differential operator is defined by using weak partial derivatives as follows:

$$\mathcal{L}_w(\sigma) = \boldsymbol{\mu} \cdot \nabla_w\sigma + \frac{1}{2}\sum_{i,j=1}^{d} a_{ij}\partial^2_{ji,w}\sigma$$

for any $\sigma \in V_{h,k}$.

Let us introduce the following bilinear forms:

$$s(\rho, \sigma) = \sum_{T\in\mathcal{T}_h} s_T(\rho, \sigma), \qquad \rho, \sigma \in V_{h,k},$$

$$b(\sigma, v) = \sum_{T\in\mathcal{T}_h} b_T(\sigma, v), \qquad \sigma \in V_{h,k},\ v \in W_{h,s},$$

Copyright © by SIAM. Unauthorized reproduction of this article is prohibited.

where

$$
\begin{aligned}
s_T(\rho,\sigma) = & h_T^{-3}\int_{\partial T}(\rho_0-\rho_b)(\sigma_0-\sigma_b)ds \\
& + h_T^{-1}\int_{\partial T}(\nabla\rho_0-\boldsymbol{\rho}_g)(\nabla\sigma_0-\boldsymbol{\sigma}_g)ds \\
& + \gamma\int_T \mathcal{L}(\rho_0)\mathcal{L}(\sigma_0)dT
\end{aligned} \tag{4.1}
$$

and

$$
b_T(\sigma,v) = (v,\mathcal{L}_w(\sigma))_T.
$$

Here, $\gamma \geq 0$ is a parameter independent of the meshsize h and the functions involved.

We are now in a position to state our primal-dual weak Galerkin finite element scheme for the model variational problem (2.3).

PRIMAL-DUAL WEAK GALERKIN ALGORITHM 4.1. *Let $k \geq 1$ be a given integer and $s \geq 0$ be another integer. A numerical approximation for the solution of* (2.3) *is the component u_h in $(u_h;\rho_h) \in W_{h,s}\times V_{h,k}^0$ satisfying*

$$
s(\rho_h,\sigma) + b(\sigma,u_h) = -(f,\sigma_0) \qquad \forall\sigma\in V_{h,k}^0, \tag{4.2}
$$

$$
b(\rho_h,v) = 0 \qquad \forall v\in W_{h,s}. \tag{4.3}
$$

5. Solution existence, uniqueness, and stability. The goal of this section is to study the solution for the numerical scheme (4.2)–(4.3). In particular, we shall prove the existence and uniqueness for the numerical solution under certain assumptions on the finite element partition $\mathcal{T}_h$ and the differential operator $\mathcal{L}$.

On each element $T \in \mathcal{T}_h$, denote by Q_0 the L^2 projection onto $P_k(T)$, $k \geq 1$. Similarly, on each edge or face $e \subset \partial T$, denote by Q_b and $\mathbf{Q}_g := (Q_{g1},\ldots,Q_{gd})$ the L^2 projections onto $P_k(e)$ and $[P_{k-1}(e)]^d$, respectively. For any $w \in H^2(\Omega)$, define the projection $Q_h w \in V_{h,k}$ so that on each element T one has

$$
Q_h w = \{Q_0 w, Q_b w, \mathbf{Q}_g(\nabla w)\}. \tag{5.1}
$$

Denote by $\mathcal{Q}_h^{(s)}$ the L^2 projection onto $W_{h,s}$—the space of piecewise polynomials of degree $s \geq 0$. In the rest of this paper, the integer s will be taken as either $s = k-1$ or $s = k-2$.

LEMMA 5.1 (see [37, 38, 41]). *The aforementioned projection operators satisfy the following commutative properties: For any $w \in H^2(T)$, one has*

$$
\partial_{ij,w}^2(Q_h w) = \mathcal{Q}_h^{(s)}\left(\partial_{ij}^2 w\right), \qquad i,j = 1,\ldots,d, \tag{5.2}
$$

$$
\nabla_w(Q_h w) = \mathcal{Q}_h^{(k-1)}(\nabla w). \tag{5.3}
$$

Proof. For any $\varphi \in P_s(T)$ and $w \in H^2(T)$, from (3.3), the usual property of L^2 projections, and the integration by parts, we have

$$
\begin{aligned}
\left(\partial_{ij,w}^2(Q_h w),\varphi\right)_T &= \left(Q_0 w,\partial_{ji}^2\varphi\right)_T - \langle Q_b w,\partial_j\varphi\cdot n_i\rangle_{\partial T} + \langle Q_{gi}(\partial_i w)\cdot n_j,\varphi\rangle_{\partial T} \\
&= \left(w,\partial_{ji}^2\varphi\right)_T - \langle w,\partial_j\varphi\cdot n_i\rangle_{\partial T} + \langle \partial_i w\cdot n_j,\varphi\rangle_{\partial T} \\
&= \left(\partial_{ij}^2 w,\varphi\right)_T \\
&= \left(\mathcal{Q}_h^{(s)}\partial_{ij}^2 w,\varphi\right)_T,
\end{aligned}
$$

which completes the proof of (5.2). The other identity (5.3) can be derived in a similar fashion, and details can be found in [37, 38, 41]. ∎

Copyright © by SIAM. Unauthorized reproduction of this article is prohibited.

Downloaded 12/18/20 to 59.64.129.2. Redistribution subject to SIAM license or copyright; see https://epubs.siam.org/page/terms

Downloaded 12/18/20 to 59.64.129.2. Redistribution subject to SIAM license or copyright; see https://epubs.siam.org/page/terms

For any element $T \in \mathcal{T}_h$, the oscillation of a function $\eta = \eta(x) \in L^\infty(\Omega)$ on T is defined as

$$\mathrm{osc}(\eta, T) := \operatorname*{essen\,sup}_{x,y\in T} |\eta(x) - \eta(y)|.$$

The local oscillation of $\eta = \eta(x)$ with respect to the partition $\mathcal{T}_h$ is defined by

$$\mathrm{osc}(\eta, \mathcal{T}_h) := \max_{T\in\mathcal{T}_h} \mathrm{osc}(\eta, T).$$

DEFINITION 5.2. *For a given nonnegative integer m, a function $\eta = \eta(x) \in L^\infty(\Omega)$ is said to be uniformly piecewise C^m with respect to the partition $\mathcal{T}_h$ if $\eta|_T \in W^{m,\infty}(T)$ for each $T \in \mathcal{T}_h$. Furthermore, for any given $\varepsilon > 0$, there exists a $\delta > 0$ such that*

$$\mathrm{osc}(\partial^s \eta, \mathcal{T}_h) < \epsilon, \qquad 0 \le |s| = s_1 + s_2 \le m$$

whenever $h < \delta$. Here $s = (s_1, s_2)$ is a multi-index and $\partial^s = \partial_x^{s_1}\partial_y^{s_2}$ is the corresponding partial derivative.

The stabilizer $s(\cdot,\cdot)$ defined through (4.1) naturally induces a seminorm in the weak finite element space $V_{h,k}$ as follows:

$$|\!|\!|\rho|\!|\!|_w = s(\rho,\rho)^{\frac{1}{2}}, \qquad \rho \in V_{h,k}. \tag{5.4}$$

LEMMA 5.3 (inf-sup condition). *Assume that the drift term $\boldsymbol{\mu} \in L^\infty(\Omega)$ and the coefficient tensor $a(x)$ is uniformly piecewise continuous with respect to the finite element partition $\mathcal{T}_h$. Then, there exists a constant $\beta > 0$ such that for any $v \in W_{h,s}$, there exists a weak function $\sigma \in V_{h,k}^0$ satisfying*

$$b(v,\sigma) \ge \frac{1}{2}\|v\|^2, \tag{5.5}$$

$$|\!|\!|\sigma|\!|\!|_w \le \beta\|v\|, \tag{5.6}$$

provided that meshsize satisfies $h \le h_0$ for a small but fixed parameter value $h_0 > 0$.

Proof. Let Φ be the solution of the following auxiliary problem:

$$\mathcal{L}\Phi = v \qquad \text{in } \Omega, \tag{5.7}$$

$$\Phi = 0 \qquad \text{on } \partial\Omega. \tag{5.8}$$

From assumption (2.4), the problem (5.7)–(5.8) has the following H^2-regularity estimate:

$$\|\Phi\|_2 \le C\|v\|. \tag{5.9}$$

With $\sigma = Q_h\Phi$, we have from Lemma 5.1 that

$$\begin{aligned} b(v,\sigma) &= \sum_{T\in\mathcal{T}_h} (v, \mathcal{L}_w(Q_h\Phi))_T \\ &= \sum_{T\in\mathcal{T}_h} (\boldsymbol{\mu} v, \nabla_w Q_h\Phi)_T + \frac{1}{2}\sum_{i,j=1}^d \left(a_{ij}v, \partial^2_{ji,w} Q_h\Phi\right)_T \\ &= \sum_{T\in\mathcal{T}_h} \left(\boldsymbol{\mu} v, \mathcal{Q}_h^{(k-1)}(\nabla\Phi)\right)_T + \frac{1}{2}\sum_{i,j=1}^d \left(a_{ij}v, \mathcal{Q}_h^{(s)}\partial^2_{ji}\Phi\right)_T \end{aligned} \tag{5.10}$$

Copyright © by SIAM. Unauthorized reproduction of this article is prohibited.

$$
\begin{aligned}
&= \sum_{T\in\mathcal{T}_h} (\boldsymbol{\mu} v, \nabla\Phi)_T + \frac{1}{2}\sum_{i,j=1}^{d} \left(a_{ij} v, \partial_{ji}^2 \Phi\right)_T \\
&\quad + \left(\boldsymbol{\mu} v, \left(\mathcal{Q}_h^{(k-1)} - I\right)\nabla\Phi\right)_T + \frac{1}{2}\sum_{i,j=1}^{d} \left(a_{ij} v, \left(\mathcal{Q}_h^{(s)} - I\right)\partial_{ji}^2\Phi\right)_T \\
&= \sum_{T\in\mathcal{T}_h} (v, v)_T + \sum_{T\in\mathcal{T}_h} \left(\boldsymbol{\mu} v, \left(\mathcal{Q}_h^{(k-1)} - I\right)\nabla\Phi\right)_T \\
&\quad + \frac{1}{2}\sum_{i,j=1}^{d} \left(\left(a_{ij} - \bar{a}_{ij}\right) v, \left(\mathcal{Q}_h^{(s)} - I\right)\partial_{ij}^2\Phi\right)_T,
\end{aligned}
$$

where $\bar{a}_{ij}$ stands for the average of a_{ij} on each element $T \in \mathcal{T}_h$. As the coefficient tensor $a(x) = (a_{ij}(x))_{d\times d}$ is uniformly piecewise continuous in Ω, there exists a small parameter $\varepsilon(h)$ depending on the meshsize h and the continuity of a_{ij} on each element T such that

$$
\begin{aligned}
&\left|\sum_{T\in\mathcal{T}_h} \left(\boldsymbol{\mu} v, \left(\mathcal{Q}_h^{(k-1)} - I\right)\nabla\Phi\right)_T\right| \le Ch\|\Phi\|_2\|v\|, \\
&\left|\sum_{i,j=1}^{d} \left(\left(a_{ij} - \bar{a}_{ij}\right) v, \left(\mathcal{Q}_h^{(s)} - I\right)\partial_{ij}^2\Phi\right)_T\right| \le C\varepsilon(h)\|\Phi\|_2\|v\|.
\end{aligned}
$$

Substituting the above estimates into (5.10) yields

$$
\begin{aligned}
b(v,\sigma) &\ge \|v\|^2 - C(h+\varepsilon(h))\|\Phi\|_2\|v\| \\
&\ge (1 - Ch - C\varepsilon(h))\|v\|^2,
\end{aligned} \tag{5.11}
$$

where we have used the regularity estimate (5.9). In particular, for $\varepsilon_0 = \frac{1}{2C}$, there exists a parameter value h_0 such that $h + \varepsilon(h) \le \varepsilon_0$ when $h \le h_0$. It follows that $(h+\varepsilon(h))C \le \frac{1}{2}$ holds true for $h \le h_0$, and hence

$$
b(v,\sigma) \ge \frac{1}{2}\|v\|^2, \tag{5.12}
$$

which verifies the inequality (5.5).

It remains to establish the estimate (5.6) for $\sigma = Q_h\Phi$. To this end, from the usual trace inequality we have

$$
\begin{aligned}
&\sum_{T\in\mathcal{T}_h} h_T^{-3}\int_{\partial T} |\sigma_0 - \sigma_b|^2 ds \\
&\quad = \sum_{T\in\mathcal{T}_h} h_T^{-3}\int_{\partial T} |Q_0\Phi - Q_b\Phi|^2 ds \\
&\quad \le \sum_{T\in\mathcal{T}_h} h_T^{-3}\int_{\partial T} |Q_0\Phi - \Phi|^2 ds \\
&\quad \lesssim \sum_{T\in\mathcal{T}_h} h_T^{-4}\int_{T} |Q_0\Phi - \Phi|^2 dT + h_T^{-2}\int_T |\nabla Q_0\Phi - \nabla\Phi|^2 dT \\
&\quad \lesssim \|\Phi\|_2^2 \lesssim \|v\|^2.
\end{aligned} \tag{5.13}
$$

Copyright © by SIAM. Unauthorized reproduction of this article is prohibited.

Downloaded 12/18/20 to 59.64.129.2. Redistribution subject to SIAM license or copyright; see https://epubs.siam.org/page/terms

Downloaded 12/18/20 to 59.64.129.2. Redistribution subject to SIAM license or copyright; see https://epubs.siam.org/page/terms

A similar analysis can be applied to yield the following estimate:

$$\sum_{T\in\mathcal{T}_h} h_T^{-1}\int_{\partial T}|\nabla\sigma_0-\boldsymbol{\sigma}_g|^2ds\lesssim\|v\|^2. \tag{5.14}$$

Furthermore, we have

$$\begin{aligned}\sum_{T\in\mathcal{T}_h}\gamma\int_T|\mathcal{L}(\sigma_0)|^2dT&\lesssim\sum_{T\in\mathcal{T}_h}\|\sigma_0\|_{2,T}^2\\&\lesssim\sum_{T\in\mathcal{T}_h}\|Q_0\Phi\|_{2,T}^2\\&\lesssim\|\Phi\|_2^2\lesssim\|v\|^2.\end{aligned} \tag{5.15}$$

Finally, by combining the estimates (5.13)–(5.15) and the definition of $|||\sigma|||_w$ we obtain

$$|||\sigma|||_w^2\le\beta^2\|v\|^2$$

for some constant β. This completes the proof of the lemma. ∎

We are now in a position to state the main result on solution existence and uniqueness.

THEOREM 5.4. *Assume that the drift vector $\boldsymbol{\mu}$ and the coefficient tensor $a(x)$ are uniformly piecewise continuous in Ω with respect to the finite element partition $\mathcal{T}_h$. Under the H^2-regularity assumption* (2.4)*, there exists a fixed $h_0>0$ such that the primal-dual weak Galerkin finite element algorithm* (4.2)–(4.3) *has one and only one solution if the meshsize satisfies $h\le h_0$.*

Proof. It suffices to show that zero is the only solution to the problem (4.2)–(4.3) with homogeneous data $f=0$. To this end, assume $f=0$ in (4.2)–(4.3). By choosing $v=u_h$ and $\sigma=\rho_h$, the difference of (4.3) and (4.2) gives $s(\rho_h,\rho_h)=0$, which implies $\rho_0=\rho_b$ and $\nabla\rho_0=\boldsymbol{\rho}_g$ on each ∂T, and hence $\rho_0\in C_0^1(\Omega)$.

For $\gamma>0$, it follows from $s(\rho_h,\rho_h)=0$ that $\mathcal{L}(\rho_0)=0$ on each element $T\in\mathcal{T}_h$. This shows that $\rho_0\in C_0^1(\Omega)$ and satisfies

$$\mathcal{L}\rho_0=0\qquad\text{in }\Omega.$$

From the H^2 regularity assumption (2.4) for the differential operator $\mathcal{L}$ with homogeneous Dirichlet boundary condition, we obtain $\rho_0\equiv0$, and hence $\rho_h\equiv0$.

As to the case of $\gamma=0$, note that (4.3) implies $Q_h^{(s)}\mathcal{L}_w(\rho_h)=0$. Since $\rho_0\in C_0^1(\Omega)$, then the weak derivatives of ρ_h up to order 2 coincide with the strong derivatives. It follows that $\rho_0\in C_0^1(\Omega)$ satisfies

$$Q_h^{(s)}\mathcal{L}(\rho_0)=0\qquad\text{in }\Omega.$$

Thus, we have

$$\begin{aligned}\mathcal{L}(\rho_0)&=\left(I-Q_h^{(s)}\right)\mathcal{L}(\rho_0)\\&=\left(I-Q_h^{(s)}\right)\left(\frac{1}{2}\sum_{i,j=1}^d a_{ij}\partial_{ji}^2\rho_0+\boldsymbol{\mu}\cdot\nabla\rho_0\right)\end{aligned} \tag{5.16}$$

Copyright © by SIAM. Unauthorized reproduction of this article is prohibited.

$$= \left(I - Q_h^{(s)}\right)\left(\frac{1}{2}\sum_{i,j=1}^{d}(a_{ij}-\bar{a}_{ij})\partial_{ji}^2\rho_0 + \boldsymbol{\mu}\cdot\nabla\rho_0 - \bar{\boldsymbol{\mu}}\cdot\overline{\nabla\rho_0)}\right)$$

$$= \left(I - Q_h^{(s)}\right)\left(\frac{1}{2}\sum_{i,j=1}^{d}(a_{ij}-\bar{a}_{ij})\partial_{ji}^2\rho_0 + (\boldsymbol{\mu}-\bar{\boldsymbol{\mu}})\cdot\nabla\rho_0 + \bar{\boldsymbol{\mu}}\cdot(\nabla\rho_0 - \overline{\nabla\rho_0)})\right).$$

From the piecewise continuity assumption on the coefficient tensor $a(x)$ and the drift vector $\boldsymbol{\mu}$, there exist a constant C and a parameter $\varepsilon(h)$ such that

$$\|\mathcal{L}\rho_0\| \le (\varepsilon(h) + Ch)\|\rho_0\|_2,$$

where $\varepsilon(h) \to 0$ as $h \to 0$. Combining the above estimate with the H^2-regularity assumption (2.4) we obtain

$$\|\rho_0\|_2 \lesssim \|\mathcal{L}\rho_0\| \le (\varepsilon(h) + Ch)\|\rho_0\|_2,$$

which implies $\rho_0 \equiv 0$, and hence $\rho_h \equiv 0$ for sufficiently small h.

With $\rho_h = 0$, (4.2) now becomes

$$b(u_h, \tau) = 0 \qquad \forall \tau \in V_{h,k}^0. \tag{5.17}$$

From Lemma 5.3, there exists a $\sigma \in V_{h,k}^0$ such that $b(u_h, \sigma) \ge \frac{1}{2}\|u_h\|^2$. It then follows from (5.17) that $u_h \equiv 0$. This completes the proof of the theorem. ∎

6. Error equations. In this section we shall derive an error equation for the numerical solution arising from the primal-dual weak Galerkin finite element algorithm (4.2)–(4.3). To this end, let u and $(u_h; \rho_h) \in W_{h,s} \times V_{h,k}^0$ be the solution of (2.3) and (4.2)–(4.3), respectively. Note that ρ_h is supposed to approximate the trivial function $\rho = 0$.

LEMMA 6.1. *For any $\sigma \in V_{h,k}$ and $v \in W_{h,s}$, the following identity holds true:*

$$(\mathcal{L}_w\sigma, v)_T = (\mathcal{L}\sigma_0, v)_T + R_T(\sigma, v), \tag{6.1}$$

where

$$\begin{aligned} R_T(\sigma, v) = {} & \frac{1}{2}\sum_{i,j=1}^{d}\left\langle \sigma_0 - \sigma_b, n_j\partial_i\left(\mathcal{Q}_h^{(s)}(a_{ij}v)\right)\right\rangle_{\partial T} \\ & - \frac{1}{2}\sum_{i,j=1}^{d}\left\langle \partial_j\sigma_0 - \sigma_{gj}, n_i\mathcal{Q}_h^{(s)}(a_{ij}v)\right\rangle_{\partial T} \\ & - \left\langle \sigma_0 - \sigma_b, \mathcal{Q}_h^{(k-1)}(\boldsymbol{\mu}v)\cdot\mathbf{n}\right\rangle_{\partial T}. \end{aligned} \tag{6.2}$$

Proof. From the formula (3.4) and (3.6) for the weak derivatives, we have

$$\begin{aligned} & (\mathcal{L}_w(\sigma), v)_T \\ & = (\boldsymbol{\mu}\cdot\nabla_w\sigma, v)_T + \frac{1}{2}\sum_{i,j=1}^{d}\left(a_{ij}\partial_{ji,w}^2\sigma, v\right)_T \\ & = \left(\nabla_w\sigma, \mathcal{Q}_h^{(k-1)}(\boldsymbol{\mu}v)\right)_T + \frac{1}{2}\sum_{i,j=1}^{d}\left(\partial_{ji,w}^2\sigma, \mathcal{Q}_h^{(s)}(a_{ij}v)\right)_T \end{aligned} \tag{6.3}$$

Copyright © by SIAM. Unauthorized reproduction of this article is prohibited.

Downloaded 12/18/20 to 59.64.129.2. Redistribution subject to SIAM license or copyright; see https://epubs.siam.org/page/terms

$$= (\nabla\sigma_0, \boldsymbol{\mu} v)_T + \frac{1}{2}\sum_{i,j=1}^{d} \left(\partial_{ji}^2 \sigma_0, a_{ij} v\right)_T + R_T(\sigma, v)$$
$$= (\mathcal{L}\sigma_0, v)_T + R_T(\sigma, v),$$

where $R_T(\sigma, v)$ is given by (6.2). ∎

By *error functions* we mean the difference between the numerical solution and the L^2 interpolation of the exact solution, namely,

$$e_h = u_h - \mathcal{Q}_h^{(s)} u, \tag{6.4}$$
$$\epsilon_h = \rho_h - Q_h\rho = \rho_h. \tag{6.5}$$

LEMMA 6.2. *Let u and $(u_h; \rho_h) \in W_{h,s} \times V_{h,k}^0$ be the solutions arising from* (1.3) *and* (4.2)–(4.3)*, respectively. Assume that the drift vector $\boldsymbol{\mu}$ and the coefficient tensor $a(x)$ are uniformly piecewise continuous in Ω with respect to the finite element partition $\mathcal{T}_h$. Then, the error functions e_h and ϵ_h satisfy the equations*

$$s(\epsilon_h, \sigma) + b(\sigma, e_h) = \ell_u(\sigma) \qquad \forall \sigma \in V_{h,k}^0, \tag{6.6}$$
$$b(\epsilon_h, v) = 0 \qquad \forall v \in W_{h,s}, \tag{6.7}$$

where $\ell_u(\sigma)$ is given by

$$\begin{aligned}
\ell_u(\sigma) = &\sum_{T\in\mathcal{T}_h} \left\langle \sigma_b - \sigma_0, \left(\boldsymbol{\mu} u - \mathcal{Q}_h^{(k-1)}\left(\boldsymbol{\mu}\mathcal{Q}_h^{(s)} u\right)\right)\cdot \mathbf{n}\right\rangle_{\partial T} \\
&+ \frac{1}{2}\sum_{T\in\mathcal{T}_h}\sum_{i,j=1}^{d} \left\langle \sigma_0 - \sigma_b, n_j \partial_i \left(a_{ij} u - \mathcal{Q}_h^{(s)}\left(a_{ij}\mathcal{Q}_h^{(s)} u\right)\right)\right\rangle_{\partial T} \\
&- \frac{1}{2}\sum_{T\in\mathcal{T}_h}\sum_{i,j=1}^{d} \left\langle \left(\partial_j\sigma_0 - \sigma_{gj}\right) n_i, a_{ij} u - \mathcal{Q}_h^{(s)}\left(a_{ij}\mathcal{Q}_h^{(s)} u\right)\right\rangle_{\partial T} \\
&+ \sum_{T\in\mathcal{T}_h} \left(\mathcal{L}(\sigma_0), \mathcal{Q}_h^{(s)} u - u\right)_T .
\end{aligned} \tag{6.8}$$

Note that the trace of a_{ij} and $\boldsymbol{\mu}$ is well defined on ∂T under the assumption of the uniform piecewise continuity for the coefficients.

Proof. First of all, from (6.5) and (4.3) we have

$$b(\epsilon_h, v) = b(\rho_h, v) = 0 \qquad \forall v \in W_{h,s},$$

which gives (6.7).

Next, notice that $\rho = 0$. Thus, by using (4.2) we arrive at

$$\begin{aligned}
&s(\rho_h - Q_h\rho, \sigma) + b\left(\sigma, u_h - \mathcal{Q}_h^{(s)} u\right) \\
&\quad = s(\rho_h, \sigma) + b(\sigma, u_h) - b\left(\sigma, \mathcal{Q}_h^{(s)} u\right) \\
&\quad = -\left(f, \sigma_0\right) - b\left(\sigma, \mathcal{Q}_h^{(s)} u\right).
\end{aligned} \tag{6.9}$$

The rest of the proof shall deal with the term $b(\sigma, \mathcal{Q}_h^{(s)} u)$. To this end, we use Lemma 6.1 to obtain

Downloaded 12/18/20 to 59.64.129.2. Redistribution subject to SIAM license or copyright; see https://epubs.siam.org/page/terms

Copyright © by SIAM. Unauthorized reproduction of this article is prohibited.

$$
\begin{aligned}
b\left(\sigma, \mathcal{Q}_h^{(s)} u\right) &= \sum_{T\in\mathcal{T}_h} \left(\mathcal{L}_w \sigma, \mathcal{Q}_h^{(s)} u\right)_T \\
&= \sum_{T\in\mathcal{T}_h} \left(\mathcal{L}\sigma_0, \mathcal{Q}_h^{(s)} u\right)_T + R_T\left(\sigma, \mathcal{Q}_h^{(s)} u\right) \\
&= \sum_{T\in\mathcal{T}_h} (\mathcal{L}\sigma_0, u)_T + \left(\mathcal{L}\sigma_0, \mathcal{Q}_h^{(s)} u - u\right)_T + R_T\left(\sigma, \mathcal{Q}_h^{(s)} u\right).
\end{aligned} \tag{6.10}
$$

From the integration by parts we have

$$
\begin{aligned}
\sum_{T\in\mathcal{T}_h} (\mathcal{L}\sigma_0, u)_T &= \sum_{T\in\mathcal{T}_h} \left((\boldsymbol{\mu}\cdot\nabla\sigma_0, u)_T + \frac{1}{2}\sum_{i,j=1}^{d} \left(a_{ij}\partial_{ji}^2\sigma_0, u\right)_T \right) \\
&= \sum_{T\in\mathcal{T}_h} \left(\sigma_0, -\nabla\cdot(\boldsymbol{\mu}u) + \frac{1}{2}\sum_{i,j=1}^{d} \partial_{ij}^2(a_{ij}u) \right)_T \\
&\quad + \sum_{T\in\mathcal{T}_h} \left\langle \sigma_0, \boldsymbol{\mu}u\cdot\mathbf{n} - \frac{1}{2}\sum_{i,j=1}^{d} n_j\partial_i(a_{ij}u) \right\rangle_{\partial T} \\
&\quad + \sum_{T\in\mathcal{T}_h}\sum_{j=1}^{d} \left\langle \partial_j\sigma_0, \frac{1}{2}\sum_{i=1}^{d} a_{ij}n_i u \right\rangle_{\partial T}.
\end{aligned} \tag{6.11}
$$

As u is the exact solution of (2.3) and $\sigma_b = 0$ on $\partial\Omega$, we then have

$$
\sum_{T\in\mathcal{T}_h} \left\langle \sigma_b, \boldsymbol{\mu}u\cdot\mathbf{n} - \frac{1}{2}\sum_{i,j=1}^{d} n_j\partial_i(a_{ij}u) \right\rangle_{\partial T} = 0, \tag{6.12}
$$

$$
\sum_{T\in\mathcal{T}_h}\sum_{j=1}^{d} \left\langle \sigma_{gj}, \frac{1}{2}\sum_{i=1}^{d} a_{ij}n_i u \right\rangle_{\partial T} = 0. \tag{6.13}
$$

By combining (6.11) with (6.12) and (6.13) we arrive at

$$
\begin{aligned}
\sum_{T\in\mathcal{T}_h} (\mathcal{L}\sigma_0, u)_T = &-(\sigma_0, f) + \sum_{T\in\mathcal{T}_h} \left\langle \sigma_0 - \sigma_b, \boldsymbol{\mu}u\cdot\mathbf{n} - \frac{1}{2}\sum_{i,j=1}^{d} n_j\partial_i(a_{ij}u) \right\rangle_{\partial T} \\
&+ \sum_{T\in\mathcal{T}_h}\sum_{j=1}^{d} \left\langle \partial_j\sigma_0 - \sigma_{gj}, \frac{1}{2}\sum_{i=1}^{d} a_{ij}n_i u \right\rangle_{\partial T}.
\end{aligned} \tag{6.14}
$$

Finally, substituting (6.14) and (6.10) into (6.9) gives rise to the error equation (6.6) after regrouping the remaining terms. This completes the proof of the lemma. ∎

7. Error estimates. The goal of this section is to establish an error estimate for the numerical solutions arising from the primal-dual weak Galerkin finite element scheme (4.2)–(4.3). The key to our error analysis is the error equation (6.6)–(6.7) and the inf-sup condition (5.5)–(5.6) that will be employed to estimate the primal variable.

In what follows, we use the standard notation of $\delta_{i,j}$ for the Kronecker delta having value 1 if $i = j$ and value 0 otherwise. The following is the main theoretical result.

Copyright © by SIAM. Unauthorized reproduction of this article is prohibited.

Downloaded 12/18/20 to 59.64.129.2. Redistribution subject to SIAM license or copyright; see https://epubs.siam.org/page/terms

Downloaded 12/18/20 to 59.64.129.2. Redistribution subject to SIAM license or copyright; see https://epubs.siam.org/page/terms

THEOREM 7.1. *Let u and $(u_h;\rho_h) \in W_{h,s} \times V_{h,k}^0$ be the solutions of* (2.3) *and* (4.2)–(4.3) *with stabilization parameter $\gamma > 0$. Assume that the coefficient tensor $a(x)$ and the drift vector $\boldsymbol{\mu}$ are uniformly piecewise smooth up to order $s+1$ in Ω with respect to the finite element partition $\mathcal{T}_h$ that is shape regular* [41]. *In addition, assume that the exact solution u satisfies $u \in \prod_{T\in T_h} H^{s+1}(T) \cap H^2(T)$. Then, the following estimate holds true:*

(7.1)
$$|||\rho_h|||_w + \|u_h - \mathcal{Q}_h^{(s)}u\| \lesssim h^k\|u\|_{k-1} + h^{s+1}\left(1+\gamma^{-1/2}\right)\|u\|_{s+1} + h^{s+2}\delta_{k,2}\|u\|_2,$$

provided that $h < h_0$ for a sufficiently small but fixed $h_0 > 0$. Here the derivatives in the Sobolev norms are taken locally on each element of $\mathcal{T}_h$.

Proof. Recall that $s = k-2$ or $s = k-1$ is the degree of polynomials employed to approximate the primal variable u. By letting $\sigma = \epsilon_h$ in the error equation (6.6) and using (6.7) we arrive at

$$s(\epsilon_h, \epsilon_h) = \ell_u(\epsilon_h). \tag{7.2}$$

To deal with the term on the right-hand side of (7.2), we use the Cauchy–Schwarz inequality, the representation (6.8), and the estimates (9.5)–(9.8) to obtain

$$\begin{aligned}
&|\ell_u(\sigma)| \\
&\le \left(\sum_{T\in\mathcal{T}_h} h_T^{-3}\|\sigma_0-\sigma_b\|_{\partial T}^2\right)^{\frac12}\left(\sum_{T\in\mathcal{T}_h} h_T^3\left\|\left(\boldsymbol{\mu}u - \mathcal{Q}_h^{(k-1)}\left(\boldsymbol{\mu}\mathcal{Q}_h^{(s)}u\right)\right)\cdot\mathbf{n}\right\|_{\partial T}^2\right)^{\frac12} \\
&\quad + \left(\sum_{T\in\mathcal{T}_h}\sum_{j=1}^d h_T^{-3}\|\sigma_0-\sigma_b\|_{\partial T}^2\right)^{\frac12}\left(\sum_{T\in\mathcal{T}_h}\sum_{i,j=1}^d h_T^3\left\|\partial_i\left(a_{ij}u - \mathcal{Q}_h^{(s)}\left(a_{ij}\mathcal{Q}_h^{(s)}u\right)\right)\right\|_{\partial T}^2\right)^{\frac12} \\
&\quad + \left(\sum_{T\in\mathcal{T}_h}\sum_{j=1}^d h_T^{-1}\|\partial_j\sigma_0-\sigma_{gj}\|_{\partial T}^2\right)^{\frac12}\left(\sum_{T\in\mathcal{T}_h}\sum_{i,j=1}^d h_T\left\|a_{ij}u - \mathcal{Q}_h^{(s)}\left(a_{ij}\mathcal{Q}_h^{(s)}u\right)\right\|_{\partial T}^2\right)^{\frac12} \\
&\quad + \left(\sum_{T\in\mathcal{T}_h}\|\mathcal{L}(\sigma_0)\|_T^2\right)^{\frac12}\left(\sum_{T\in\mathcal{T}_h}\|\mathcal{Q}_h^{(s)}u-u\|_T^2\right)^{\frac12} \\
&\lesssim h^k\|u\|_{k-1}|||\sigma|||_w + h^{s+1}(\|u\|_{s+1}+h\delta_{k,2}\|u\|_2)|||\sigma|||_w \\
&\quad + h^{s+1}\|u\|_{s+1}|||\sigma|||_w + h^{s+1}\gamma^{-1/2}\|u\|_{s+1}|||\sigma|||_w \\
&\lesssim \left(h^k\|u\|_{k-1} + h^{s+1}\left(1+\gamma^{-1/2}\right)\|u\|_{s+1} + h^{s+2}\delta_{k,2}\|u\|_2\right)|||\sigma|||_w
\end{aligned}$$

for any $\sigma \in V_{h,k}^0$. Now substituting the above estimate into (7.2) yields the error estimate

$$|||\epsilon_h|||_w^2 \lesssim \left(h^k\|u\|_{k-1} + h^{s+1}\left(1+\gamma^{-1/2}\right)\|u\|_{s+1} + h^{s+2}\delta_{k,2}\|u\|_2\right)|||\epsilon_h|||_w,$$

which leads to

$$|||\epsilon_h|||_w \lesssim h^k\|u\|_{k-1} + h^{s+1}\left(1+\gamma^{-1/2}\right)\|u\|_{s+1} + h^{s+2}\delta_{k,2}\|u\|_2. \tag{7.3}$$

Next, for the error function $e_h = u_h - \mathcal{Q}_h^{(s)}u$, from the inf-sup condition (5.5)–(5.6) there exists a $\sigma \in V_{h,k}^0$ such that

Copyright © by SIAM. Unauthorized reproduction of this article is prohibited.

$$\frac{1}{2}\|e_h\|^2 \le |b(e_h,\sigma)|, \quad |||\sigma|||_w \le \beta\|e_h\|. \tag{7.4}$$

On the other hand, the error equation (6.6) implies

$$b(e_h,\sigma) = \ell_u(\sigma) - s(\epsilon_h,\sigma).$$

It follows that

$$\begin{aligned} |b(e_h,\sigma)| &\le |\ell_u(\sigma)| + |||\epsilon_h|||_w |||\sigma|||_w \\ &\lesssim \left(h^k\|u\|_{k-1} + h^{s+1}\left(1+\gamma^{-1/2}\right)\|u\|_{s+1} + h^{s+2}\delta_{k,2}\|u\|_2\right)|||\sigma|||_w. \end{aligned} \tag{7.5}$$

Combing (7.4) with (7.5) gives rise to the error estimate

$$\frac{1}{2}\|e_h\|^2 \lesssim \left(h^k\|u\|_{k-1} + h^{s+1}\left(1+\gamma^{-1/2}\right)\|u\|_{s+1} + h^{s+2}\delta_{k,2}\|u\|_2\right)\|e_h\|,$$

which leads to

$$\|e_h\| \lesssim h^k\|u\|_{k-1} + h^{s+1}\left(1+\gamma^{-1/2}\right)\|u\|_{s+1} + h^{s+2}\delta_{k,2}\|u\|_2. \tag{7.6}$$

The error estimate (7.1) is a direct result of (7.3) and (7.6). This completes the proof of the theorem. ∎

From the usual triangle inequality and the error estimate (7.1), we have the following estimate for the numerical approximation of the primal variable.

COROLLARY 7.2. *Under the assumptions of Theorem* 7.1*, one has the following optimal order error estimate in the* L^2 *norm:*

$$\|u-u_h\| \lesssim h^k\|u\|_{k-1} + h^{s+1}\left(1+\gamma^{-1/2}\right)\|u\|_{s+1} + h^{s+2}\delta_{k,2}\|u\|_2. \tag{7.7}$$

The case of piecewise constant for $a(x)$ and the drift vector $\boldsymbol{\mu}$ deserves special consideration in the error analysis since the term $\ell(\sigma)$ in (6.8) can be simplified by using the fact that $(\mathcal{L}(\sigma_0), \mathcal{Q}_h^{(s)}u - u)_T = 0$ if $s = k-1$. In particular, the stabilization term $\gamma\int_T \mathcal{L}(\rho_0)\mathcal{L}(\sigma_0)dT$ in (4.1) is no longer needed in the numerical scheme. A mathematical theory for this special, yet useful, case can be established by slightly modifying the proof of Theorem 7.1. The result is stated as follows without proof.

THEOREM 7.3. *Let* u *and* $(u_h;\rho_h) \in W_{h,k-1}\times V_{h,k}^0$ *be the solutions of* (2.3) *and* (4.2)–(4.3) *with stabilization parameter* $\gamma \ge 0$*. Assume that the coefficient tensor* $a(x)$ *and the drift vector* $\boldsymbol{\mu}$ *are piecewise constant with respect to the shape regular finite element partition* $\mathcal{T}_h$*. Assume that the exact solution* u *satisfies* $u \in \prod_{T\in T_h} H^k(T)$*,* $k \ge 2$*. Then, the error estimate*

$$|||\rho_h|||_w + \|u_h - u\| \lesssim h^k\|u\|_k \tag{7.8}$$

hold true, provided that the meshsize h *is sufficiently small. Here the derivatives in the Sobolev norm are taken locally on each element of* $\mathcal{T}_h$*.*

In Table 7.1, we provide a summary for the rate of convergence for the numerical approximation u_h arising from the Weak Galerkin scheme (4.2)–(4.3). The first line of the table indicates the type of elements used in the numerical scheme. Recall that the space $W_{h,s}$ was employed for approximating u_h, while $V_{h,k}$ was for the auxiliary variable ρ_h. Although the solution u_h is the quantity of major interest in this application, we believe that the auxiliary variable ρ_h might provide some useful information for the design of error estimators for u_h. The second row of the table shows an optimal order of convergence for u_h in the usual L^2-norm, i.e., a convergence of order k when piecewise polynomials of degree $k-1$ are used.

Copyright © by SIAM. Unauthorized reproduction of this article is prohibited.

Downloaded 12/18/20 to 59.64.129.2. Redistribution subject to SIAM license or copyright; see https://epubs.siam.org/page/terms

TABLE 7.1
Convergence for the primal-dual weak Galerkin finite element method.

	$V_{h,k} \times W_{h,k-2},\ k \geq 2$	$V_{h,k} \times W_{h,k-1},\ k \geq 1$
$\|u - u_h\|$	h^{k-1}	h^k

8. C^0-type elements and computational complexity. By C^0-type elements, we mean a special class of finite element spaces $V_{h,k}$ consisting of weak finite element functions $v = \{v_0, v_b, \mathbf{v}_g\}$, where $v_b = v_0|_{\partial T}$ on each element $T \in \mathcal{T}_h$. Analogously, C^{-1}-type elements refer to the general case of $v = \{v_0, v_b, \mathbf{v}_g\} \in V_{h,k}$ for which v_b is totally independent of v_0. It is clear that C^0-type finite element schemes involve fewer degrees of freedom than C^{-1}-type, as the boundary component v_b can obviously be eliminated from the list of unknowns. However, C^0-type elements would impose some limitations on the geometry of the finite element partition $\mathcal{T}_h$. For the C^{-1}-type elements, all the unknowns corresponding to v_0 can be eliminated locally on each element through a condensation process before assembling the global stiffness matrix. Table 8.1 shows the degrees of freedom on triangular elements, and Table 8.2 contains similar data on tetrahedra.

The error estimates shown in Theorem 7.1 can be extended to C^0-type triangular elements for $V_{h,k}$. The rest of this section explains some modifications necessary for such an extension. First of all, for C^0-type elements, the discrete weak second order partial derivative $\partial^2_{ij,w} v$ can be computed as a polynomial in $P_s(T)$ on each element T by the following equation:

$$\left(\partial^2_{ij,w} v, \varphi\right)_T = -(\partial_i v_0, \partial_j \varphi)_T + \langle v_{gi}, \varphi n_j \rangle_{\partial T} \qquad \forall \varphi \in P_s(T). \tag{8.1}$$

For the convergence analysis to work, we need to have the error equations (6.6)–(6.7), which in turn require the commutative property (5.2)–(5.3) for a properly defined projection operator Q_h given as in (5.1). As there is no change on the variable $\mathbf{v}_g$ and the space it lives in, the operator $\mathbf{Q}_g$ should remain unchanged as the usual L^2 projection into the space of polynomials of degree $k-1$ on each piece of ∂T. However, the operator Q_0 must be modified by using the interpolation operator $\tilde{I}_k$ given as

TABLE 8.1
The degrees of freedom for the element $V_k(T) \times P_{k-2}(T),\ k \geq 2$, on triangles.

	$V_k(T)$			$P_{k-2}(T)$
	v_0	v_b	$\mathbf{v}_g$	
C^{-1}-type	$\frac{1}{2}(k+1)(k+2)$	$3(k+1)$	$6k$	$\frac{1}{2}(k-1)k$
C^0-type	$\frac{1}{2}(k+1)(k+2)$	0	$6k$	$\frac{1}{2}(k-1)k$
Hybridized C^{-1}	0	$3(k+1)$	$6k$	$\frac{1}{2}(k-1)k$

TABLE 8.2
The degrees of freedom for the element $V_k(T) \times P_{k-2}(T),\ k \geq 2$, on tetrahedra.

	$V_k(T)$			$P_{k-2}(T)$
	v_0	v_b	$\mathbf{v}_g$	–
C^{-1}-type	$\frac{1}{6}(k+1)(k+2)(k+3)$	$2(k+1)(k+2)$	$6k(k+1)$	$\frac{1}{6}(k^2-1)k$
C^0-type	$\frac{1}{6}(k+1)(k+2)(k+3)$	0	$6k(k+1)$	$\frac{1}{6}(k^2-1)k$
Hybridized C^{-1}	0	$2(k+1)(k+2)$	$6k(k+1)$	$\frac{1}{6}(k^2-1)k$

Copyright © by SIAM. Unauthorized reproduction of this article is prohibited.

Downloaded 12/18/20 to 59.64.129.2. Redistribution subject to SIAM license or copyright; see https://epubs.siam.org/page/terms

Downloaded 12/18/20 to 59.64.129.2. Redistribution subject to SIAM license or copyright; see https://epubs.siam.org/page/terms

in Lemma A.3 of [20]. For two-dimensional triangular elements, this interpolating polynomial $\tilde{I}_k v \in P_k(T)$ satisfies

$$\int_e (v - \tilde{I}_k v)\phi ds = 0 \quad \forall\ \phi \in P_{k-2}(e), \quad \forall \text{ side } e \text{ of } T, \tag{8.2}$$

$$\int_T (v - \tilde{I}_k v)\phi ds = 0 \quad \forall\ \phi \in P_{k-3}(T). \tag{8.3}$$

From the integration by parts, (8.2), and (8.3), we then obtain

$$\begin{aligned} (\partial_i \tilde{I}_k v, \partial_j \varphi)_T &= -(\tilde{I}_k v, \partial^2_{ji}\varphi)_T + \langle \tilde{I}_k v, \partial_j \varphi n_i\rangle_{\partial T} \\ &= -(v, \partial^2_{ji}\varphi)_T + \langle v, \partial_j \varphi n_i\rangle_{\partial T} \\ &= (\partial_i v, \partial_j \varphi)_T \end{aligned} \tag{8.4}$$

for all $\varphi \in P_{k-1}(T)$. Thus, from (8.1), (8.4), and the fact that $s \le k-1$ we arrive at

$$\begin{aligned} \left(\partial^2_{ij,w} Q_h v, \varphi\right)_T &= -(\partial_i \tilde{I}_k v, \partial_j \varphi)_T + \langle (\mathbf{Q}_g \nabla v)_i, \varphi n_j\rangle_{\partial T} \\ &= -(\partial_i v, \partial_j \varphi)_T + \langle (\nabla v)_i, \varphi n_j\rangle_{\partial T} \\ &= \left(\partial^2_{ij} v, \varphi\right)_T \\ &= \left(\mathcal{Q}_h \partial^2_{ij} v, \varphi\right)_T \end{aligned}$$

for all $\varphi \in P_s(T)$, which implies the commutative property (5.2). Note that (5.3) clearly holds true as the weak gradient is identical with the strong gradient for C^0-type elements. Readers are encouraged to check out [26] for a detailed discussion on the use of C^0-type elements in the context of weak Galerkin finite element methods.

9. Error estimates for L^2 projections. Recall that $\mathcal{T}_h$ is a shape regular finite element partition of the domain Ω. For any $T \in \mathcal{T}_h$ and $\phi \in H^1(T)$, the following trace inequality holds true [41]:

$$\|\phi\|^2_{\partial T} \lesssim h_T^{-1}\|\phi\|^2_T + h_T \|\nabla \phi\|^2_T. \tag{9.1}$$

If ϕ is a polynomial on the element $T \in \mathcal{T}_h$, then from the inverse inequality, we have [41]

$$\|\phi\|^2_{\partial T} \lesssim h_T^{-1}\|\phi\|^2_T. \tag{9.2}$$

LEMMA 9.1. *Let $\mathcal{T}_h$ be a finite element partition of Ω satisfying the shape regular assumption given in* [41]. *For $0 \le t \le \min(2, k)$, the following estimates hold true:*

$$\sum_{T\in\mathcal{T}_h} h_T^{2t}\|u - Q_0 u\|^2_{t,T} \lesssim h^{2(m+1)}\|u\|^2_{m+1}, \qquad m \in [t-1, k],\ k \ge 1, \tag{9.3}$$

$$\sum_{T\in\mathcal{T}_h} h_T^{2t}\|u - \mathcal{Q}_h^{(k-1)} u\|^2_{t,T} \lesssim h^{2m}\|u\|^2_{m}, \qquad m \in [t, k],\ k \ge 1, \tag{9.4}$$

$$\sum_{T\in\mathcal{T}_h} h_T^{2t}\|u - \mathcal{Q}_h^{(k-2)} u\|^2_{t,T} \lesssim h^{2m}\|u\|^2_{m}, \qquad m \in [t, k-1],\ k \ge 2. \tag{9.5}$$

Note that (9.5) *is merely a different form of* (9.4).

LEMMA 9.2. *In addition to the assumptions of Lemma* 9.1, *assume that the coefficient tensor $a(x)$ and the drift vector $\boldsymbol{\mu}$ are uniformly piecewise smooth up to*

Copyright © by SIAM. Unauthorized reproduction of this article is prohibited.

order $m-1$ in Ω with respect to the finite element partition $\mathcal{T}_h$. Then for any $v \in \prod_{T\in\mathcal{T}_h} H^{m-1}(T) \cap H^2(T)$, the following estimates hold true:

$$\left(\sum_{T\in\mathcal{T}_h} h_T^3 \left\| \left(\boldsymbol{\mu} v - \mathcal{Q}_h^{(k-1)} \left(\boldsymbol{\mu} \mathcal{Q}_h^{(s)} v \right) \right) \cdot \mathbf{n} \right\|_{\partial T}^2 \right)^{\frac{1}{2}} \lesssim h^m \|v\|_{m-1}; \tag{9.6}$$

$$\begin{aligned} &\left(\sum_{T\in\mathcal{T}_h} \sum_{i,j=1}^{d} h_T^3 \left\| \partial_i \left(a_{ij} v - \mathcal{Q}_h^{(s)} \left(a_{ij} \mathcal{Q}_h^{(s)} v \right) \right) \right\|_{\partial T}^2 \right)^{\frac{1}{2}} \\ &\qquad \lesssim h^{m-1} (\|v\|_{m-1} + h\delta_{m,2} \|v\|_2); \end{aligned} \tag{9.7}$$

$$\left(\sum_{T\in\mathcal{T}_h} \sum_{i,j=1}^{d} h_T \left\| a_{ij} u - \mathcal{Q}_h^{(s)} \left(a_{ij} \mathcal{Q}_h^{(s)} u \right) \right\|_{\partial T}^2 \right)^{\frac{1}{2}} \lesssim h^{m-1} \|u\|_{m-1}. \tag{9.8}$$

Here, m is an integer satisfying $m \in [2, k+1]$ if $s = k-1$ and $m \in [2,k]$ if $s = k-2$.

Proof. To prove (9.6), from the trace inequality (9.1) and the estimate (9.5) we have

$$\begin{aligned} &\sum_{T\in\mathcal{T}_h} h_T^3 \left\| \left(\boldsymbol{\mu} v - \mathcal{Q}_h^{(k-1)} \left(\boldsymbol{\mu} \mathcal{Q}_h^{(s)} v \right) \right) \cdot \mathbf{n} \right\|_{\partial T}^2 \\ &\quad \lesssim \sum_{T\in\mathcal{T}_h} h_T^2 \left\| \boldsymbol{\mu} v - \mathcal{Q}_h^{(k-1)} \left(\boldsymbol{\mu} \mathcal{Q}_h^{(s)} v \right) \right\|_T^2 + h_T^4 \left\| \boldsymbol{\mu} v - \mathcal{Q}_h^{(k-1)} \left(\boldsymbol{\mu} \mathcal{Q}_h^{(s)} v \right) \right\|_{1,T}^2 \\ &\quad \lesssim \sum_{T\in\mathcal{T}_h} h_T^2 \left\| \boldsymbol{\mu} v - \mathcal{Q}_h^{(k-1)} (\boldsymbol{\mu} v) \right\|_T^2 + h_T^2 \left\| \mathcal{Q}_h^{(k-1)} (\boldsymbol{\mu} v) - \mathcal{Q}_h^{(k-1)} \left(\boldsymbol{\mu} \mathcal{Q}_h^{(s)} v \right) \right\|_T^2 \\ &\qquad + h_T^4 \left\| \boldsymbol{\mu} v - \mathcal{Q}_h^{(k-1)} (\boldsymbol{\mu} v) \right\|_{1,T}^2 + h_T^4 \left\| \mathcal{Q}_h^{(k-1)} (\boldsymbol{\mu} v) - \mathcal{Q}_h^{(k-1)} \left(\boldsymbol{\mu} \mathcal{Q}_h^{(s)} v \right) \right\|_{1,T}^2 \\ &\quad \lesssim \sum_{T\in\mathcal{T}_h} h_T^2 \left\| \boldsymbol{\mu} v - \mathcal{Q}_h^{(k-1)} (\boldsymbol{\mu} v) \right\|_T^2 + h_T^2 \left\| \boldsymbol{\mu} v - \boldsymbol{\mu} \mathcal{Q}_h^{(s)} v \right\|_T^2 \\ &\qquad + h_T^4 \left\| \boldsymbol{\mu} v - \mathcal{Q}_h^{(k-1)} (\boldsymbol{\mu} v) \right\|_{1,T}^2 + h_T^4 \left\| \boldsymbol{\mu} v - \boldsymbol{\mu} \mathcal{Q}_h^{(s)} v \right\|_{1,T}^2 \\ &\quad \lesssim \ h^{2m} \|v\|_{m-1}^2 \end{aligned}$$

for $m \in [2, k+1]$ when $s = k-1$ and $m \in [2,k]$ when $s = k-2$.

As to (9.7), we use the trace inequality (9.1) and the estimate (9.5) to obtain

$$\begin{aligned} &\sum_{T\in\mathcal{T}_h} \sum_{i,j=1}^{d} h_T^3 \left\| \partial_i \left(a_{ij} v - \mathcal{Q}_h^{(s)} \left(a_{ij} \mathcal{Q}_h^{(s)} v \right) \right) \right\|_{\partial T}^2 \\ &\quad \lesssim \sum_{T\in\mathcal{T}_h} \sum_{i,j=1}^{d} h_T^2 \left\| \partial_i \left(a_{ij} v - \mathcal{Q}_h^{(s)} \left(a_{ij} \mathcal{Q}_h^{(s)} v \right) \right) \right\|_T^2 + h_T^4 \| \partial_i \left(a_{ij} v - \mathcal{Q}_h^{(s)} \left(a_{ij} \mathcal{Q}_h^{(s)} v \right) \right) \|_{1,T}^2 \\ &\quad \lesssim \sum_{T\in\mathcal{T}_h} \sum_{i,j=1}^{d} h_T^2 \left\| \partial_i \left(a_{ij} v - \mathcal{Q}_h^{(s)} (a_{ij} v) \right) \right\|_T^2 + h_T^2 \left\| \partial_i \left(\mathcal{Q}_h^{(s)} (a_{ij} v) - \mathcal{Q}_h^{(s)} \left(a_{ij} \mathcal{Q}_h^{(s)} v \right) \right) \right\|_T^2 \\ &\qquad + h_T^4 \left\| \partial_i \left(a_{ij} v - \mathcal{Q}_h^{(s)} (a_{ij} v) \right) \right\|_{1,T}^2 + h_T^4 \left\| \partial_i \left(\mathcal{Q}_h^{(s)} (a_{ij} v) - \mathcal{Q}_h^{(s)} \left(a_{ij} \mathcal{Q}_h^{(s)} v \right) \right) \right\|_{1,T}^2 \\ &\quad \lesssim \ h^{2m-2} \left(\|v\|_{m-1}^2 + h^2 \delta_{m,2} \|v\|_2^2 \right) \end{aligned}$$

for $m \in [2, k+1]$ when $s = k-1$ and $m \in [2,k]$ when $s = k-2$.

Copyright © by SIAM. Unauthorized reproduction of this article is prohibited.

Downloaded 12/18/20 to 59.64.129.2. Redistribution subject to SIAM license or copyright; see https://epubs.siam.org/page/terms

Downloaded 12/18/20 to 59.64.129.2. Redistribution subject to SIAM license or copyright; see https://epubs.siam.org/page/terms

Finally for (9.8), we again use the trace inequality (9.1) and the estimate (9.5) to obtain

$$\begin{aligned}
&\sum_{T\in\mathcal{T}_h}\sum_{i,j=1}^{d} h_T \left\|a_{ij}v - \mathcal{Q}_h^{(s)}\left(a_{ij}\mathcal{Q}_h^{(s)}v\right)\right\|_{\partial T}^2 \\
&\quad\lesssim \sum_{T\in\mathcal{T}_h}\sum_{i,j=1}^{d} \left\|a_{ij}v - \mathcal{Q}_h^{(s)}\left(a_{ij}\mathcal{Q}_h^{(s)}v\right)\right\|_T^2 + h_T^2\left\|a_{ij}v - \mathcal{Q}_h^{(s)}\left(a_{ij}\mathcal{Q}_h^{(s)}v\right)\right\|_{1,T}^2 \\
&\quad\lesssim \sum_{T\in\mathcal{T}_h}\sum_{i,j=1}^{d} \left\|a_{ij}v - \mathcal{Q}_h^{(s)}(a_{ij}v)\right\|_T^2 + \left\|\mathcal{Q}_h^{(s)}(a_{ij}v) - \mathcal{Q}_h^{(s)}\left(a_{ij}\mathcal{Q}_h^{(s)}v\right)\right\|_T^2 \\
&\qquad + h_T^2\left\|a_{ij}v - \mathcal{Q}_h^{(s)}(a_{ij}v)\right\|_{1,T}^2 + h_T^2\left\|\mathcal{Q}_h^{(s)}(a_{ij}v) - \mathcal{Q}_h^{(s)}\left(a_{ij}\mathcal{Q}_h^{(s)}v\right)\right\|_{1,T}^2 \\
&\quad\lesssim \sum_{T\in\mathcal{T}_h}\sum_{i,j=1}^{d} \left\|a_{ij}v - \mathcal{Q}_h^{(s)}(a_{ij}v)\right\|_T^2 + \left\|a_{ij}v - a_{ij}\mathcal{Q}_h^{(s)}v\right\|_T^2 \\
&\qquad + h_T^2\left\|a_{ij}v - \mathcal{Q}_h^{(s)}(a_{ij}v)\right\|_{1,T}^2 + h_T^2\left\|a_{ij}v - a_{ij}\mathcal{Q}_h^{(s)}v\right\|_{1,T}^2 \\
&\quad\lesssim\ h^{2m-2}\|v\|_{m-1}^2,
\end{aligned}$$

where $m\in[2,k+1]$ if $s=k-1$ and $m\in[2,k]$ if $s=k-2$. This completes the proof of the lemma. ∎

10. Numerical results. The goal of this section is to present some numerical results for the finite element scheme (4.2)–(4.3). Our test problem seeks u satisfying

$$\begin{aligned}
\nabla\cdot(\boldsymbol{\mu}u) - \frac{1}{2}\sum_{i,j=1}^{d}\partial_{ij}^2(a_{ij}u) &= f \quad \text{in } \Omega, \\
u &= g \quad \text{on } \partial\Omega,
\end{aligned} \tag{10.1}$$

where Ω is a polygonal domain in two-dimensions. As the problem (10.1) has nonhomogeneous Dirichlet data on the boundary, the weak formulation (2.3) must be modified accordingly so that the weak solution $u=u(x)\in L^2(\Omega)$ is given by the following equation:

$$\int_\Omega u\mathcal{L}(v)dx = \frac{1}{2}\sum_{i,j=1}^{d}\int_{\partial\Omega} g a_{ij}n_i\partial_j v ds - \int_\Omega f v dx \qquad \forall v\in H^2(\Omega)\cap H_0^1(\Omega). \tag{10.2}$$

The corresponding primal-dual weak Galerkin finite element scheme seeks $(u_h;\rho_h)\in W_{h,s}\times V_{h,k}^0$ satisfying

$$s(\rho_h,\sigma) + b(\sigma,u_h) = \frac{1}{2}\sum_{i,j=1}^{d}\langle a_{ij}g,\sigma_{gj}n_i\rangle_{\partial\Omega} - (f,\sigma_0), \qquad \forall\sigma\in V_{h,k}^0, \tag{10.3}$$

$$b(\rho_h,v) = 0 \qquad \forall v\in W_{h,s}. \tag{10.4}$$

Our numerical implementation is based on the primal-dual weak Galerkin scheme (10.3)–(10.4) with the element of order $k=2$ on uniformly triangular finite element partitions. This configuration corresponds to the following selection for the finite element spaces:

$$V_{h,2} = \{\rho=\{\rho_0,\rho_b,\boldsymbol{\rho}_g\}:\ \rho_0\in P_2(T),\rho_b\in P_2(e),\boldsymbol{\rho}_g\in[P_1(e)]^2, e\subset\partial T, T\in\mathcal{T}_h\}$$

Copyright © by SIAM. Unauthorized reproduction of this article is prohibited.

and

$$W_{h,s} = \{w : \ w|_T \in P_s(T), \ \forall T \in \mathcal{T}_h\} \quad s = 0 \text{ or } 1.$$

For simplicity, our numerical experiments will be conducted for only C^0-type elements for which ρ_b is identical with the trace of ρ_0 on ∂T for any $T \in \mathcal{T}_h$. For convenience, the C^0-type weak Galerkin element with $s = 1$ (i.e., $W_{h,1}$) shall be called the $P_2(T)/[P_1(\partial T)]^2/P_1(T)$ element. Analogously, the case corresponding to $s = 0$ (i.e., $W_{h,0}$) is called $P_2(T)/[P_1(\partial T)]^2/P_0(T)$.

Two polygonal domains are considered in the numerical experiments, with the first one being the unit square $\Omega = (0,1)^2$ and the second an L-shaped region with vertices $A_0 = (0,0), \ A_1 = (2,0), \ A_2 = (2,1), \ A_3 = (1,1), \ A_4 = (1,2)$, and $A_5 = (0,2)$. Note that the error estimates developed in the previous section are applicable to the square domain but not to the L-shaped domain. Nevertheless, our primal-dual weak Galerkin finite element scheme is well formulated on any domains. The L-shaped domain is chosen just for the purposes of demonstrating the performance of the algorithm for cases for which theory has not been developed.

The finite element partitions in our computation are obtained through a simple uniform refinement procedure as follows. Given an initial coarse triangulation of the domain, a sequence of triangulations are obtained successively through a uniform refinement that divides each coarse level triangle into four congruent subtriangles by connecting the three midpoints on the edges. We use $\rho_h = \{\rho_0, \boldsymbol{\rho}_g\} \in V_{h,2}$ and $u_h \in W_{h,s}, \ s = 0, 1$, to denote the numerical solutions arising from (4.2)–(4.3). The numerical solutions are compared with carefully chosen interpolations of the exact solution in various norms. In particular, the primal variable u_h is compared with the exact solution u on each element at either three vertices (for $s = 1$) or the center (for $s = 0$), which is known as the nodal point interpolation and is denoted as $I_h u$. The auxiliary variable ρ_h is supposed to approximate the true solution $\rho = 0$ and is therefore compared with $Q_h \rho = 0$. The error functions are thus denoted as

$$\epsilon_h = \rho_h - Q_h \rho \equiv \{\rho_0, \boldsymbol{\rho}_g\}, \quad e_h = u_h - I_h u.$$

The following norms are applied in the computation for the error:

$$L^2\text{- norm:} \quad |\!|\!|\rho_h|\!|\!|_0 = \left(\sum_{T \in \mathcal{T}_h} \int_T |\rho_0|^2 dT \right)^{\frac{1}{2}},$$

$$\text{semi } H^1\text{-norm:} \quad |\!|\!|\boldsymbol{\rho}_h|\!|\!|_1 = \left(\sum_{T \in \mathcal{T}_h} h_T \int_{\partial T} |\boldsymbol{\rho}_g|^2 ds \right)^{\frac{1}{2}},$$

$$L^2\text{-norm:} \quad \|e_h\|_0 = \left(\sum_{T \in \mathcal{T}_h} \int_T |e_h|^2 dT \right)^{\frac{1}{2}}.$$

Tables 10.1–10.2 illustrate the performance of the C^0-type $P_2(T)/[P_1(\partial T)]^2/P_1(T)$ element for the test problem (10.1) with exact solution given by $u = \sin(x_1)\sin(x_2)$ on the unit square domain and the L-shaped domain. The right-hand-side function and the Dirichlet boundary condition are chosen to match the exact solution. Our numerical results indicate that the convergence rate for the solution u_h is of order $r = 2$ in the discrete L^2-norm on both the unit square domain and the L-shaped domain. The result is in great consistency with the theoretical rate of convergence for u_h on the square domain. The computational results are equally good for the L-shaped domain in the absence of a mathematical theory.

Copyright © by SIAM. Unauthorized reproduction of this article is prohibited.

Downloaded 12/18/20 to 59.64.129.2. Redistribution subject to SIAM license or copyright; see https://epubs.siam.org/page/terms

TABLE 10.1

Numerical rates of convergence for the C^0-$P_2(T)/[P_1(\partial T)]^2/P_1(T)$ element applied to problem (10.1) with exact solution $u = \sin(x_1)\sin(x_2)$ on $\Omega = (0,1)^2$; the coefficient matrix $a_{11} = 3$, $a_{12} = a_{21} = 1$, and $a_{22} = 2$; the drift vector $\boldsymbol{\mu} = [1,1]$; the stabilizer parameter $\gamma = 0$.

$1/h$	$\|\rho_h\|_0$	Order	$\|\boldsymbol{\rho}_g\|_1$	Order	$\|u_h - I_h u\|_0$	Order
1	3.52e-01		4.02e-00		2.11e-01	
2	4.09e-02	3.11	7.16e-01	2.49	5.55e-02	1.93
4	3.77e-03	3.44	1.22e-01	2.55	1.42e-02	1.97
8	2.78e-04	3.76	1.79e-02	2.79	3.57e-03	1.99
16	1.87e-05	3.90	2.36e-03	2.91	8.93e-04	2.00
32	1.20e-06	3.95	3.04e-04	2.96	2.23e-04	2.00

TABLE 10.2

Numerical rates of convergence for the C^0-$P_2(T)/[P_1(\partial T)]^2/P_1(T)$ element applied to the problem (10.1) with exact solution $u = \sin(x_1)\sin(x_2)$ on the L-shaped domain; the coefficient matrix $a_{11} = 3$, $a_{12} = a_{21} = 1$, and $a_{22} = 2$; the drift vector $\boldsymbol{\mu} = [1,1]$; the stabilizer parameter $\gamma = 0$.

$1/h$	$\|\rho_h\|_0$	Order	$\|\boldsymbol{\rho}_g\|_1$	Order	$\|u_h - I_h u\|_0$	Order
1	5.33e-01		5.20e-00		3.07e-01	
2	7.77e-02	2.78	1.18e-00	2.15	8.03e-02	1.94
4	6.42e-03	3.60	1.90e-01	2.63	2.04e-02	1.98
8	4.49e-04	3.84	2.65e-02	2.84	5.11e-03	2.00
16	2.95e-05	3.93	3.47e-03	2.93	1.27e-03	2.00
32	1.89e-06	3.97	4.44e-04	2.97	3.18e-04	2.00

TABLE 10.3

Numerical rates of convergence for the C^0-$P_2(T)/[P_1(\partial T)]^2/P_0(T)$ element applied to the problem (10.1) with exact solution $u = \sin(x_1)\sin(x_2)$ on $\Omega = (0,1)^2$; the coefficient matrix $a_{11} = 3$, $a_{12} = a_{21} = 1$, and $a_{22} = 2$; the drift vector $\boldsymbol{\mu} = [1,1]$; the stabilizer parameter $\gamma = 0$.

$1/h$	$\|\rho_h\|_0$	Order	$\|\boldsymbol{\rho}_g\|_1$	Order	$\|u_h - I_h u\|_0$	Order
1	9.82e-03		2.57e-01		1.03e-01	
2	4.79e-03	1.04	6.98e-02	1.88	4.38e-02	1.23
4	1.53e-03	1.65	1.81e-02	1.95	1.72e-02	1.35
8	3.76e-04	2.02	4.43e-03	2.03	7.74e-03	1.15
16	9.27e-05	2.02	1.09e-03	2.02	3.77e-03	1.04
32	2.31e-05	2.01	2.72e-04	2.01	1.87e-03	1.01

TABLE 10.4

Convergence rates for the C^0-$P_2(T)/[P_1(\partial T)]^2/P_0(T)$ element applied to problem (10.1) with exact solution $u = \sin(x_1)\sin(x_2)$ on the L-shaped domain; the coefficient matrix is $a_{11} = 3$, $a_{12} = a_{21} = 1$, and $a_{22} = 2$; the drift vector $\boldsymbol{\mu} = [1,1]$; the stabilizer parameter $\gamma = 0$.

$1/h$	$\|\rho_h\|_0$	Order	$\|\boldsymbol{\rho}_g\|_1$	Order	$\|u_h - I_h u\|_0$	Order
1	0.0199		5.01e-01		1.72e-01	
2	0.0165	0.269	1.39e-01	1.85	7.65e-02	1.17
4	0.00470	1.81	3.60e-02	1.95	3.37e-02	1.18
8	1.18E-03	2.00	8.96e-03	2.01	1.61e-02	1.07
16	2.93E-04	2.01	2.23e-03	2.01	7.92e-03	1.02
32	7.32E-05	2.00	5.56e-04	2.00	3.94e-03	1.01

Tables 10.3–10.4 illustrate the performance of the C^0-type $P_2(T)/[P_1(\partial T)]^2/P_0(T)$ element for the test problem (10.1) with exact solution given by $u = \sin(x_1)\sin(x_2)$ on the unit square domain and the L-shaped domain with constant coefficients. The numerical results are in good consistency with what the theory predicts for convex domains.

Downloaded 12/18/20 to 59.64.129.2. Redistribution subject to SIAM license or copyright; see https://epubs.siam.org/page/terms

Copyright © by SIAM. Unauthorized reproduction of this article is prohibited.

Downloaded 12/18/20 to 59.64.129.2. Redistribution subject to SIAM license or copyright; see https://epubs.siam.org/page/terms

Tables 10.5–10.6 illustrate the performance of the C^0-type $P_2(T)/[P_1(\partial T)]^2/P_0(T)$ element for the test problem (10.1) on the unit square domain and the L-shaped domain. The exact solution is given by $u = \sin(x_1)\sin(x_2)$ and the differential operator has variable coefficients. The numerical rate of convergence for the primal-dual WG finite element method is consistent with the theory on the square domain. The performance of the method on the L-shaped domain is also excellent in the absence of a mathematical theory.

Tables 10.7–10.9 illustrate the performance of the C^0-type $P_2(T)/[P_1(\partial T)]^2/P_1(T)$ element for the test problem (10.1) when the parameter γ varies in the stabilizer $s(\cdot,\cdot)$. The exact solution is given by $u = \sin(x_1)\sin(x_2)$, and the domain in this test case is the unit square with constant coefficients and drifting vector. The results indicate that the convergence rate for the solution u_h of the weak Galerkin algorithm (4.2)–(4.3) is of order $r = 2$ in the discrete L^2-norm for u_h for different values of $\gamma \geq 0$. Table 10.10 illustrates the performance of the numerical scheme on the L-shaped domain with $\gamma = 10000$. It is interesting to note that the absolute error for both the primal and the dual variables decreases as γ increases. But for large values

TABLE 10.5

Numerical rates of convergence for the C^0-$P_2(T)/[P_1(\partial T)]^2/P_0(T)$ element applied to problem (10.1) with exact solution $u = \sin(x_1)\sin(x_2)$ on $\Omega = (0,1)^2$; the coefficient matrix $a_{11} = 1 + x_1^2$, $a_{12} = a_{21} = 0.25x_1x_2$, and $a_{22} = 1 + x_2^2$; the drift vector $\boldsymbol{\mu} = [x, y]$; the stabilizer parameter $\gamma = 0$.

$1/h$	$\|\rho_h\|_0$	Order	$\|\boldsymbol{\rho}_g\|_1$	Order	$\|u_h - I_h u\|_0$	Order
1	1.18e-02		1.94e-01		4.88e-02	
2	1.09e-03	3.44	4.70e-02	2.05	2.49e-02	0.97
4	3.13e-04	1.81	1.13e-02	2.05	1.14e-02	1.13
8	8.76e-05	1.83	2.77e-03	2.03	5.52e-03	1.04
16	2.25e-05	1.96	6.85e-04	2.02	2.74e-03	1.01
32	5.67e-06	2.00	1.70e-04	2.01	1.37e-03	1.00

TABLE 10.6

Numerical rates of convergence rates for the C^0-$P_2(T)/[P_1(\partial T)]^2/P_0(T)$ element applied to the problem (10.1) with exact solution $u = \sin(x_1)\sin(x_2)$ on the L-shaped domain; the coefficient matrix $a_{11} = 1 + x_1^2$, $a_{12} = a_{21} = 0.25x_1x_2$, and $a_{22} = 1 + x_2^2$; the drift vector $\boldsymbol{\mu} = [x, y]$; the stabilizer parameter $\gamma = 0$.

$1/h$	$\|\rho_h\|_0$	Order	$\|\boldsymbol{\rho}_g\|_1$	Order	$\|u_h - I_h u\|_0$	Order
1	2.12e-02		5.39e-01		2.03e-01	
2	1.25e-02	0.763	1.33e-01	2.02	9.15e-02	1.15
4	3.09e-03	2.01	3.24e-02	2.04	4.23e-02	1.11
8	7.60e-04	2.02	7.93e-03	2.03	2.06e-02	1.04
16	1.89e-04	2.01	1.96e-03	2.02	1.02e-02	1.01
32	4.71e-05	2.00	4.87e-04	2.01	5.10e-03	1.00

TABLE 10.7

Numerical rates of convergence for the C^0-$P_2(T)/[P_1(\partial T)]^2/P_1(T)$ element applied to the problem (10.1) with exact solution $u = \sin(x_1)\sin(x_2)$ on $\Omega = (0,1)^2$; the coefficient matrix $a_{11} = 3$, $a_{12} = a_{21} = 1$, and $a_{22} = 2$; the drift vector $\boldsymbol{\mu} = [1, 1]$; the stabilizer parameter $\gamma = 0.1$.

$1/h$	$\|\rho_h\|_0$	Order	$\|\boldsymbol{\rho}_g\|_1$	Order	$\|u_h - I_h u\|_0$	Order
1	2.22E-01		2.59E+00		1.40E-01	
2	2.12E-02	3.39	4.51E-01	2.52	4.58E-02	1.61
4	1.62E-03	3.71	6.74E-02	2.74	1.29E-02	1.83
8	1.09E-04	3.89	8.97E-03	2.91	3.39E-03	1.93
16	7.01E-06	3.96	1.15E-03	2.97	8.65E-04	1.97
32	4.41E-07	3.99	1.44E-04	2.99	2.18E-04	1.99

Copyright © by SIAM. Unauthorized reproduction of this article is prohibited.

TABLE 10.8
Numerical rates of convergence for the C^0-$P_2(T)/[P_1(\partial T)]^2/P_1(T)$ element applied to the problem (10.1) with exact solution $u = \sin(x_1)\sin(x_2)$ on $\Omega = (0,1)^2$; the coefficient matrix $a_{11} = 3$, $a_{12} = a_{21} = 1$, and $a_{22} = 2$; the drift vector $\boldsymbol{\mu} = [1,1]$; the stabilizer parameter $\gamma = 1.0$.

$1/h$	$\|\rho_h\|_0$	Order	$\|\boldsymbol{\rho}_g\|_1$	Order	$\|u_h - I_h u\|_0$	Order
1	5.11e-02		8.90e-01		5.58e-02	
2	8.51e-03	2.59	1.83e-01	2.28	2.20e-02	1.35
4	1.03e-03	3.04	4.41e-02	2.05	8.68e-03	1.34
8	9.02e-05	3.52	7.65e-03	2.53	2.88e-03	1.59
16	6.44e-06	3.81	1.08e-03	2.83	8.12e-04	1.82
32	4.24e-07	3.93	1.40e-04	2.94	2.13e-04	1.93

TABLE 10.9
Numerical rates of convergence for the C^0-$P_2(T)/[P_1(\partial T)]^2/P_1(T)$ element applied to the problem (10.1) with exact solution $u = \sin(x_1)\sin(x_2)$ on $\Omega = (0,1)^2$; the coefficient matrix $a_{11} = 3$, $a_{12} = a_{21} = 1$, and $a_{22} = 2$; the drift vector $\boldsymbol{\mu} = [1,1]$; the stabilizer parameter $\gamma = 10000$.

$1/h$	$\|\rho_h\|_0$	Order	$\|\boldsymbol{\rho}_g\|_1$	Order	$\|u_h - I_h u\|_0$	Order
1	5.98e-06		6.78e-01		4.04e-02	
2	1.35e-06	2.15	3.08e-02	4.46	9.48e-03	2.09
4	6.40e-07	1.08	1.39e-03	4.47	2.05e-03	2.21
8	2.26e-07	1.50	6.30e-05	4.46	4.85e-04	2.08
16	5.97e-08	1.92	6.38e-06	3.30	1.21e-04	2.01
32	1.29e-08	2.20	2.60e-06	1.30	3.15e-05	1.94

TABLE 10.10
Numerical rates of convergence for the C^0-$P_2(T)/[P_1(\partial T)]^2/P_1(T)$ element applied to the problem (10.1) with exact solution $u = \sin(x_1)\sin(x_2)$ on the L-shaped domain; the coefficient matrix $a_{11} = 3$, $a_{12} = a_{21} = 1$, and $a_{22} = 2$; the drift vector $\boldsymbol{\mu} = [1,1]$; the stabilizer parameter $\gamma = 10000$.

$1/h$	$\|\rho_h\|_0$	Order	$\|\boldsymbol{\rho}_g\|_1$	Order	$\|u_h - I_h u\|_0$	Order
1	8.31e-06		8.36e-01		1.33e-01	
2	6.90e-06	0.269	3.64e-02	4.52	2.51e-02	2.40
4	2.77e-06	1.32	1.56e-03	4.54	5.88e-03	2.09
8	7.97e-07	1.79	8.03e-05	4.28	1.45e-03	2.03
16	1.99e-07	2.00	2.11e-05	1.93	3.59e-04	2.01
32	4.35e-08	2.20	9.34e-06	1.18	8.99e-05	2.00

of the stabilization parameter γ, the rate of convergence for the dual variable seems to suffer. The numerical results are in good consistency with the theoretical predictions for small values of γ, particularly in terms of the rate of convergence for each variable. Therefore, we recommend the use of $\gamma = 1$ in practical computing. But for piecewise constant diffusive tensor and the drifting vector, Theorem 7.3 and the numerical experiments show that the stabilization γ is not necessary for the method to be convergent and accurate. In fact, we conjecture that the primal-dual finite element scheme with $\gamma = 0$ developed in this paper is stable and has optimal order of convergence for variable diffusive tensor $a(x)$ and drifting vector $\boldsymbol{\mu}$ that are uniformly piecewise continuous. Interested readers are encouraged to explore the problem with more sophisticated mathematical tools.

Figure 10.1 illustrates the performance of our numerical methods for a problem with discontinuous solution. This test problem has the following configuration: domain $\Omega = (-1,1) \times (-1,1)$, diffusion tensor $a = \alpha I$ with $\alpha = 1$ for $x_1 < 0$ and $\alpha = 2$ for $x_1 \geq 0$, load function $f = 0$, and Dirichlet boundary condition $g = 2$ for $x_1 < 0$ and $g = 1$ for $x_1 > 0$. The numerical solutions are obtained by using piecewise linear functions for the primal variable with $\gamma = 0$, i.e., $s = 1$ in the finite element space

Copyright © by SIAM. Unauthorized reproduction of this article is prohibited.

Downloaded 12/18/20 to 59.64.129.2. Redistribution subject to SIAM license or copyright; see https://epubs.siam.org/page/terms

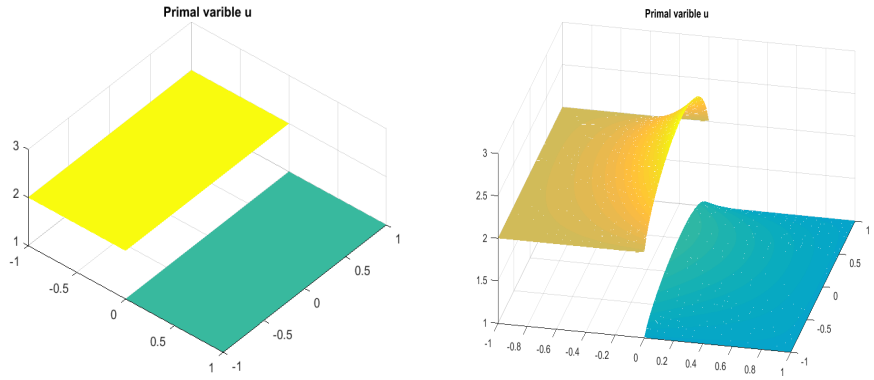

FIG. 10.1. *Domain* $\Omega = (-1,1) \times (-1,1)$, *diffusion tensor* $a = \alpha I$ *with* $\alpha = 1$ *for* $x_1 < 0$ *and* $\alpha = 2$ *for* $x_1 \geq 0$, *load function* $f = 0$, *Dirichlet boundary data* $g = 2$ *for* $x_1 < 0$ *and* $g = 1$ *for* $x_1 > 0$. *Plot for primal variable* u_h: *drift vector* $\boldsymbol{\mu} = 0$ *(left), drift vector* $\boldsymbol{\mu} = [1,1]$ *(right).*

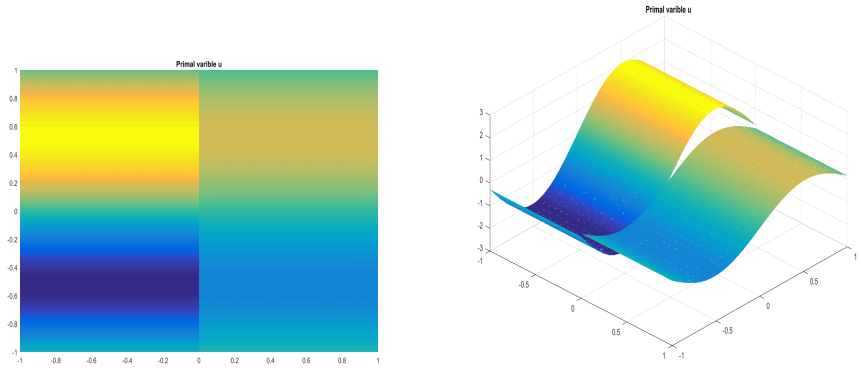

FIG. 10.2. *Domain* $\Omega = (-1,1) \times (-1,1)$, *diffusion tensor* $a = \alpha I$ *with* $\alpha = 1$ *for* $x_1 < 0$ *and* $\alpha = 2$ *for* $x_1 > 0$, *load function* $f = 9\sin(3x_2)$, *Dirichlet boudnary data* $g = 2\sin(3x_2)$ *for* $x_1 < 0$ *and* $g = \sin(3x_2)$ *for* $x_1 > 0$, *drift vector* $\boldsymbol{\mu} = 0$. *Plot for primal variable* u_h: *contour plot (left), surface plot (right).*

$W_{h,s}$. For this test problem, the exact solution is known to be $u = 2$ for $x_1 < 0$ and $u = 1$ for $x_1 > 0$ when the drift vector is zero. The plot indicates that the primal-dual weak Galerkin finite element solution is very consistent with the exact solution when $\boldsymbol{\mu} = 0$ (see the left plot). The right plot corresponds to the case of $\boldsymbol{\mu} = [1,1]$ for which no exact solution is known.

The primal-dual weak Galerkin finite element method (4.2)–(4.3) was also applied to a test problem for which the exact solution is discontinuous on the x_2-axis. The configuration of this test problem is as follows: the domain $\Omega = (-1,1) \times (-1,1)$, the diffusion coefficient $a = \alpha I$ with $\alpha = 1$ for $x_1 < 0$ and $\alpha = 2$ for $x_1 > 0$, the load function $f = 9\sin(3x_2)$, a Dirichlet boudnary value of $g = 2\sin(3x_2)$ for $x_1 < 0$ and $g = \sin(3x_2)$ for $x_1 > 0$, and the vanishing drift vector $\boldsymbol{\mu} = [0,0]$. Piecewise linear functions are used to approximate the primal variable, with the corresponding numerical solution shown in Figure 10.2. The exact solution for this test problem is given by $u = 2\sin(3x_2)$ for $x_1 < 0$ and $u = \sin(3x_2)$ for $x_1 > 0$. Table 10.11 illustrates

Copyright © by SIAM. Unauthorized reproduction of this article is prohibited.

Downloaded 12/18/20 to 59.64.129.2. Redistribution subject to SIAM license or copyright; see https://epubs.siam.org/page/terms

Downloaded 12/18/20 to 59.64.129.2. Redistribution subject to SIAM license or copyright; see https://epubs.siam.org/page/terms

TABLE 10.11

Numerical rates of convergence for the $C^0 - P_2(T)/[P_1(\partial T)]^2/P_1(T)$ element: domain $\Omega = (-1,1)\times(-1,1)$, diffusion $a = \alpha I$ with $\alpha = 1$ for $x_1 < 0$ and $\alpha = 2$ for $x_1 > 0$, load function $f = 9\sin(3x_2)$. The exact solution is given by $u = 2\sin(3x_2)$ for $x_1 < 0$ and $u = \sin(3x_2)$ for $x_1 > 0$. The drift vector is $\boldsymbol{\mu} = [0,0]$. The stabilizer parameter has value $\delta = 0$.

h^{-1}	$\|\rho_h\|_0$	Order	$\|\boldsymbol{\rho_g}\|_0$	Order	$\|u_h - I_h u\|_0$	Order
2	5.17e-00	-	4.08e+01	-	1.10e-00	-
4	4.63e-01	3.48	6.25e-00	2.71	1.80e-01	2.62
8	3.90e-02	3.57	1.09e-00	2.52	3.90e-02	2.21
16	2.74e-03	3.83	1.55e-01	2.82	9.19e-03	2.08
32	1.79e-04	3.94	2.02e-02	2.93	2.25e-03	2.03

TABLE 10.12

An example of the diffusive coefficient $a = \{a_{ij}\}_{2\times 2}$ and the value α in the exact solution formula $u = \alpha^{-1}\cos(x_1)\cos(x_2)$ on the domain $\Omega = (-1,1)^2$.

In the second quadrant: $a_{11} = 2(2 + x_1^2)$ $a_{22} = 2(2 - x_2^2)$ $\alpha = 2$	In the first quadrant: $a_{11} = 2 + x_1^2$ $a_{22} = 2 + x_2^2$ $\alpha = 1$
In the third qurdrant: $a_{11} = 3(2 - x_1^2)$ $a_{22} = 3(2 - x_2^2)$ $\alpha = 3$	In the fourth quardant: $a_{11} = 4(2 - x_1^2)$ $a_{22} = 4(2 + x_2^2)$ $\alpha = 4$

TABLE 10.13

Numerical results for the $C^0 - P_2(T)/[P_1(\partial T)]^2/P_1(T)$ element: domain $\Omega = (-1,1)^2$, diffusion coefficient $a = [a_{11}, 0; 0, a_{22}]$ defined in Table 10.12, vanishing drift vector $\boldsymbol{\mu} = [0,0]$, stabilization parameter $\delta = 0$. The exact solution is given by $u = \alpha^{-1}\cos(x_1)\cos(x_2)$.

h^{-1}	$\|\rho_h\|_0$	Order	$\|\boldsymbol{\rho_g}\|_0$	Order	$\|u_h - I_h u\|_0$	Order
1	4.58e-02	-	2.05e-01	-	5.08e-01	-
2	9.87e-03	2.21	6.96e-02	1.56	7.66e-02	2.73
4	1.17e-03	3.07	1.71e-02	2.03	1.56e-02	2.30
8	9.11e-05	3.69	2.65e-03	2.69	3.48e-03	2.16
16	6.15e-06	3.89	3.57e-04	2.89	8.32e-04	2.06
32	3.96e-07	3.96	4.59e-05	2.96	2.05e-04	2.02

the convergence performance of the numerical method, which shows an optimal order of convergence for the approximate solutions.

We further applied the numerical scheme (4.2)–(4.3) to a test problem with the following configuration: $\Omega = (-1,1)\times(-1,1)$, the diffusion matrix $a = [a_{11}, 0; 0, a_{22}]$ defined as in Table 10.12, the drift vector $\boldsymbol{\mu} = [0,0]$, and the stabilizer parameter $\delta = 0$. The exact solution is discontinuous along the x_1- and x_2-axes and is given by $u = \alpha^{-1}\cos(x_1)\cos(x_2)$, where α assumes four values shown in Table 10.12. We used piecewise linear functions to approximate the primal variable, and the numerical results are shown in Table 10.13. The results reveal optimal order of convergence for all the approximate solutions in discrete L^2 and H^1 norms.

Our last numerical experiment was conducted on a problem for which the exact solution not only is discontinuou, but is not known to us. This test problem has the following configuration: domain $\Omega = (-1,1)\times(-1,1)$, diffusion tensor $a = \alpha I$ with $\alpha = 1$ in the first and third quadrants and $\alpha = 10$ in the second and fourth quadrants, load function $f = \frac{1}{4}$, Dirichlet boundary data $g = 0$, drift vector $\boldsymbol{\mu} = [1,1]$, and stabilization parameter $\gamma = 0$. The numerical solution for the primal variable can be

Copyright © by SIAM. Unauthorized reproduction of this article is prohibited.

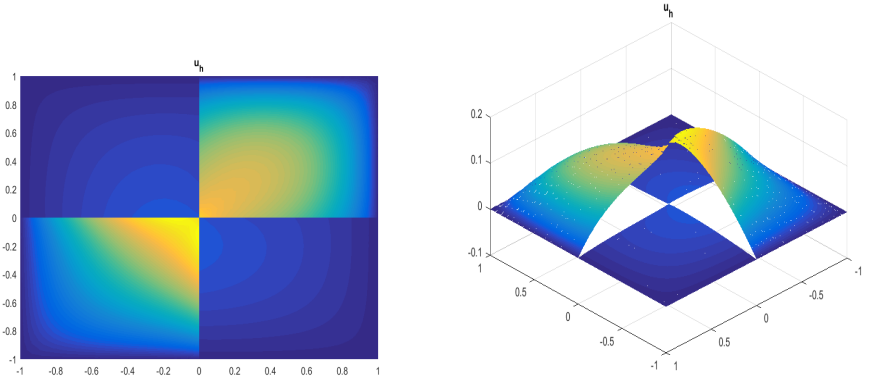

FIG. 10.3. *Domain* $\Omega = (-1,1) \times (-1,1)$*, diffusion tensor* $a = \alpha I$ *with* $\alpha = 1$ *in the first and third quadrants and* $\alpha = 10$ *in the second and fourth quadrants, load function* $f = \frac{1}{4}$*, Dirichlet boundary data* $g = 0$*, drift vector* $\boldsymbol{\mu} = [1,1]$*. Plot for primal variable* u_h*: contour plot (left), surface plot (right).*

seen in Figure 10.3. The left figure is the contour plot, and the one on the right is a three-dimensional surface plot.

REFERENCES

[1] I. BABUŠKA, *The finite element method with Lagrange multipliers*, Numer. Math., 20 (1973), pp. 179–192.

[2] L. A. BERGMAN, S. F. WOJTKIEWICZ, E. A. JOHNSON, AND B. F. SPENCER, JR., *Robust Numerical Solution of the Fokker-Planck Equation for Second Order Dynamical Systems Under Parametric and External White Noise Excitations*, Fields Inst. Commun. 9, AMS, Providence, RI, 1996.

[3] R. G. BHANDARI AND R. E. SHERRER, *Random vibrations in discrete nonlinear dynamic systems*, J. Mech. Eng. Sci., 10 (1968), pp. 168–174.

[4] S. C. BRENNER AND L. R. SCOTT, *The Mathematical Theory of Finite Element Methods*, 3rd ed., Texts Appl. Math. 15, Springer, New York, 2008.

[5] F. BREZZI, *On the existence, uniqueness, and approximation of saddle point problems arising from Lagrange multipliers*, RAIRO, 8 (1974), pp. 129–151.

[6] A. BUFFA AND P. MONK, *Error estimates for the ultra weak variational formulation of the Helmholtz equation*, ESAIM Math. Model. Numer. Anal., 42 (2008), pp. 925–940, Doi: 10.1051/m2an:2008033.

[7] E. BURMAN, *Error estimates for stabilized finite element methods applied to ill-posed problems*, C. R. Acad. Sci. Paris Ser. I, 352 (2014), pp. 655–659, http://dx.doi.org/10.1016/j.crma.2014.06.008

[8] E. BURMAN, *Stabilized finite element methods for nonsymmetric, noncoercive, and ill-possed problems. Part* I: *Elliptic equations*, SIAM J. Sci. Comput., 35 (2013), pp. A2752–A2780.

[9] E. BURMAN, *Stabilized finite element methods for nonsymmetric, noncoercive, and ill-possed problems. Part* II: *Hyperbolic equations*, SIAM J. Sci. Comput., 36 (2014), pp. A1911–A1936.

[10] O. CESSENAT AND B. DESPRÉS, *Application of an ultra weak variational formulation of elliptic PDEs to the two-dimensional Helmholtz problem*, SIAM J. Numer. Anal., 35 (1998), pp. 255–299.

[11] P.G. CIARLET, *The Finite Element Method for Elliptic Problems*, Classics in Appl. Math. 40, SIAM, Philadelphia, 2002.

[12] B. COCKBURN, J. GOPALAKRISHNAN, AND R. LAZAROV, *Unified hybridization of discontinuous Galerkin, mixed, and continuous Galerkin methods for second order elliptic problems*, SIAM J. Numer. Anal., 47 (2009), pp. 1319–1365.

[13] H. O. CORDÈS, *Zero order a priori estimates for solutions of elliptic differential equations*, in Partial Differential Equations, Proc. Sympos. Pure Math., 4, AMS, Providence, RI, 1961, pp. 157–166.

Downloaded 12/18/20 to 59.64.129.2. Redistribution subject to SIAM license or copyright; see https://epubs.siam.org/page/terms

Copyright © by SIAM. Unauthorized reproduction of this article is prohibited.

[14] L. Davis, Jr., *Modified Fermi mechanism for the acceleration of cosmic rays*, Phys. Rev., 101 (1956), pp. 351–358.
[15] B. Després, *Sur une formulation variationelle de type ultra-faible*, C. R. Acad. Sci. Paris Ser. I, 318 (1994), pp. 939–944.
[16] A. D. Fokker, *Die mittlere Energie rotierender elektrischer Dipole im Strahlungsfeld*, Ann. Phys. 348 (1914), pp. 810–820, doi:10.1002/andp.19143480507.
[17] B. X. Fraeijs de Veubeke, *Displacement and equilibrium models in the finite element method*, in Stress Analysis, O. C. Zienkiewicz and G. Holister, eds., John Wiley, New York, 1965, pp. 145–197.
[18] C. W. Gardiner, *Handbook of Stochastic Methods*, 2nd ed., Springer-Verlag, Berlin, 1985.
[19] D. Gilbarg and N. S. Trudinger. *Elliptic Partial Differential Equations of Second Order*, 2nd ed., Springer-Verlag, Berlin, 1983.
[20] V. Girault and P. A. Raviart, *Finite Element Methods for the Navier-Stokes Equations: Theory and Algorithms*, Springer-Verlag, Berlin, 1986.
[21] P. Grisvard, *Elliptic Problems in Nonsmooth Domains*, Classics in Appl. Math. 69, SIAM, Philadelphia, 2011.
[22] P. Kumar and S. Narayana, *Solution of Fokker-Planck equation by finite element and finite difference methods for nonlinear systems*, Sadhana, 31 (2006), pp. 445–461.
[23] R. S. Langley, *A finite element method for the statistics of nonlinear random vibration*, J. Sound Vibration, 101 (1985), pp. 41–54.
[24] H. P. Langtangen, *A general numerical solution method for Fokker-Planck equations with applications to structural reliability*, Probab. Engrg. Mech., 6 (1991), pp. 33–48.
[25] L. Mu, J. Wang, and X. Ye, *Weak Galerkin finite element methods on polytopal meshes*, Int. J. Numer. Anal. Model., 12 (2015), pp. 31–53.
[26] L. Mu, J. Wang, X. Ye, and S. Zhang, *A C^0-weak Galerkin finite element method for the biharmonic equation*, J. Sci. Comput., 59 (2014), pp. 473–495.
[27] A. Masud and L. A. Bergman, *Application of multi-scale finite element methods to the solution of the Fokker-Planck equation*, Comput. Methods Appl. Mech. Engrg., 194 (2005), pp. 1513–1526.
[28] B. T. Park and V. Petrosian, *Fokker-Planck equations of stochastic acceleration: A study of numerical methods*, Astrophys. J. Suppl. Ser., 103 (1996), pp. 255–267.
[29] M. Planck, *Über einen Satz der statistischen Dynamik und seine Erweiterung in der Quantentheorie*, Berlin, 1917.
[30] C. Pucci and G. Talenti, *Elliptic (second-order) partial differential equations with measurable coefficients and approximating integral equations*, Adv. Math., 19 (1976), pp. 48–105.
[31] H. Risken, *The Fokker-Planck Equation: Methods of Solution and Applications*, 2nd ed., Math. Sci. Engrg., 60, Springer-Verlag, Berlin, 1989.
[32] I. Smears and E. Süli, *Discontinuous Galerking finite element approximation of nondivergence form elliptic equations with Cordès coefficients*, SIAM J Numer. Anal., 51 (2013), pp. 2088–2106.
[33] B. F. Spencer and L. A. Bergman, *On the numerical solutions of the Fokker-Planck equations for nonlinear stochastic systems*, Nonlinear Dynam., 4 (1993), pp. 357–372.
[34] R. L. Stratonovich, *Some Markov methods in the theory of stochastic processes in nonlinear dynamical systems*, in Noise in Nonlinear Dynamical Systems, F. Moss and P. V. E. McClintock, eds., Vol. 1, Cambridge University Press, Cambridge, UK, 1989, pp. 16–68.
[35] G. Talenti, *Sopra una classe di equazioni ellittiche a coefficienti misurabili*, Ann. Mat. Pura Appl., 69 (1965), pp. 285–304.
[36] G. Talenti, *Equazioni lineari ellittiche in due variabili*, Le Matematiche, 21 (1966), pp. 339–376.
[37] C. Wang and J. Wang, *An efficient numerical scheme for the biharmonic equation by weak Galerkin finite element methods on polygonal or polyhedral meshes*, Comput. Math. Appl., 68 (2014), pp. 2314–2330, doi:10.1016/j.camwa.2014.03.021.
[38] C. Wang and J. Wang, *A hybridized weak Galerkin finite element method for the biharmonic equation*, Int. J. Numer. Anal. Model., 12 (2015), pp. 302–317.
[39] C. Wang and J. Wang, *A primal-dual weak Galerkin finite element method for second order elliptic equations in non-divergence form*, Math Comp., 87 (2018), pp. 515–545, https://doi.org/10.1090/mcom/3220.
[40] J. Wang and X. Ye, *A weak Galerkin finite element method for second-order elliptic problems*, J. Comput. Appl. Math., 241 (2013), pp. 103–115.
[41] J. Wang and X. Ye, *A weak Galerkin mixed finite element method for second-order elliptic problems*, Math. Comp., 83 (2014), pp. 2101–2126.

Downloaded 12/18/20 to 59.64.129.2. Redistribution subject to SIAM license or copyright; see https://epubs.siam.org/page/terms

Copyright © by SIAM. Unauthorized reproduction of this article is prohibited.

[42] J. Wang and X. Ye, *A weak Galerkin finite element method for the Stokes equations*, Adv. Comput. Math., 42 (2016), pp. 155–174, doi:10.1007/s10444-015-9415-2.
[43] M. F. Wheeler, *A priori L2 error estimates for Galerkin approximations to parabolic partial differential equations*, SIAM J. Numer. Anal., 10 (1973), pp. 723–759.

Downloaded 12/18/20 to 59.64.129.2. Redistribution subject to SIAM license or copyright; see https://epubs.siam.org/page/terms

Copyright © by SIAM. Unauthorized reproduction of this article is prohibited.